ELSEVIER ELSEVIER

Contents lists available at ScienceDirect

Current Opinion in Solid State & Materials Science

journal homepage: www.elsevier.com/locate/cossms





Mechanically sensing and tailoring electronic properties in two-dimensional atomic membranes

Jaehyung Yu^{a,*,1}, M. Abir Hossain^a, SunPhil Kim^{a,2}, Paolo F. Ferrari^a, Siyuan Huang^a, Yue Zhang^a, Hyunchul Kim^a, Dina A. Michel^a, Arend M. van der Zande^{a,b,*}

ARTICLE INFO

Keywords:
Nanomechanics
2D materials
Atomic membranes
Deformable electronics
Mechanically reconfigurable properties

ABSTRACT

Two-dimensional (2D) van der Waals materials are both highly deformable atomic membranes and electrically active quantum materials. Most electronic and quantum states in both monolayer 2D materials and heterostructures are highly sensitive to strain and interlayer structure, and thus may be tuned mechanically. Here we explore the current frontiers using 2D material mechanics to sense, tune, tailor or even reconfigure electronic properties, device behavior and quantum states. We compare the relative impacts of different kinds of mechanical perturbations including in-plane strain, out-of-plane vibrations, inhomogeneous three-dimensional deformations, instabilities of membranes under compression like crumpling and wrinkling, and interlayer slip. Throughout, we explore how each form of coupling may be used for applications that cannot be realized in the flat unperturbed materials including tunable nanoelectromechanical systems, strain resilient electronics, multifunctional surfaces and reconfigurable quantum systems.

1. Introduction

Two-dimensional (2D) materials are considered not only the ultimate limit of molecular electronics, but also atomically-thin mechanical membranes. Separately, both the electronic and mechanical properties of 2D materials lead to exciting new physics and applications. Yet, some of the most important research today focuses on incorporating these two properties together to create nanoscale electromechanical devices and to mechanically tune the electronic and quantum properties of the material. There is a long history in technology of using mechanics to sense and tune electronic properties. Piezoresistivity—wherein strain tunes the band structure of a material, leading to a change in density of states—is utilized in microelectromechanical systems (MEMS) such as pressure sensors. Similarly, epitaxial strain engineering is utilized to improve device performance for example to reduce inter-valley scattering, improve mobility in Si-based complementary metal--oxide-semiconductor (CMOS) transistors [1,2], and reduce hole effective mass in group III-V semiconductor lasers [3].

2D materials are particularly interesting because they host a wide

range of exotic quantum states and are able to undergo large deformations due to their atomic-scale thicknesses, opening up new routes to mechanically tune their structure. Many reviews have been written separately focusing on the electronic properties [4,5] or mechanical properties [6–8] of 2D materials, so we will not cover these topics in great detail here. Instead, this perspective will focus on the current state and future prospects of 2D material devices where both mechanics and electronics are needed to enable functionality.

2. Overview of 2D material mechanics and electronics

Outlined in as outlined in Fig. 1, the highly anisotropic layered structure of 2D materials enables diverse in-plane, out-of-plane, and interlayer mechanical deformations that can be large compared with the material dimensions. Within each layer, strong covalent bonds between atoms lead to high in-plane mechanical moduli (340 N/m per layer for graphene, equivalent to a 3D Young's modulus of 1 TPa, or about 20–100 times stronger than steel). The lack of out-of-plane dangling bonds stabilizes the 2D material, allowing them to undergo extremely

^a Department of Mechanical Science and Engineering, University of Illinois at Urbana-Champaign, Urbana, IL 61801, USA

^b Materials Research Laboratory, University of Illinois at Urbana-Champaign, Urbana, IL 61801, USA

^{*} Corresponding authors.

E-mail addresses: jaehyungyu@uchicago.edu (J. Yu), arendv@illinois.edu (A.M. van der Zande).

¹ Present address: Department of Chemistry, University of Chicago, Chicago, IL 60615, USA.

² Present address: Molecular Foundry, Lawrence Berkeley National Laboratory, Berkeley, CA 94720, USA.

large in-plane strains or shear by up to 12% before fracturing [9]. In contrast, the atomic thickness means 2D materials are extremely floppy and pliable out of plane. For example, the bending stiffness of graphene is only 1.5 eV [10], similar to a lipid bilayer of a cell membrane. However, unlike in a cell membrane where pliability is a result of fluid reconstruction, pliability in 2D materials is achieved while maintaining the crystallinity and corresponding electronic band structure, an important consideration for electronics. Finally, weak van der Waals bonds between layers cause the layers to adhere together with strength in the range of 0.23 J/m² for graphite-graphite [11,12], and do not require epitaxial matching to remain stable. However, because of the anisotropic structure, the energy barrier to shear is much lower than adhesion, 0.022 J /m² for soliton barrier height in bilayer grapheme [13]. As a result, interlayer slip is far easier than delamination. Even more intriguing, introducing twist, out of plane strain, or shear between the layers results in quasiperiodic misregistry between the layers called incommensurate Moiré superlattices [14-17]. The size of Moiré superlattices ranges from ~3 Å -20 nm [14,16,18], depending on the magnitude of twist or lattice mismatch between the different layers. At high twist angle, or at heterointerfaces, the incommensurate structures have no stable equilibrium and thus lead to ultralow friction between layers termed structural superlubricity, more than two orders magnitude lower than for aligned layers, While the numbers above are for graphene, all 2D materials share the same underlying structure and most follow similar rules.

With over 1000 members, the broad class of 2D materials also leads to diverse electronic properties and serves as an ideal platform for exploring the emergent physics in lower dimensions, with amazing discoveries in hall [26,27] and valley physics [28,29], quantum optics [30,31], and nanomagnetism [32–34]. Moreover, the adhesion and stability of 2D materials has enabled the construction of van der Waals heterostructures by stacking disparate 2D materials as molecular scale building blocks with hundreds of demonstrated applications in

molecular electronics [35]. A limited selection of examples includes high mobility transistors [36,37], atomically thin p-n junctions [38], and optical modulators [39], which demonstrate the feasibility of both in-plane and out-of-plane dominated transport in heterostructures. However, the layers cannot be treated as electrically independent. Interlayer misalignment and tuning of overlap in electronic orbitals directly tunes the electronic properties and lead to emergent quantum states. As two examples, interlayer twist tunes the band structure in bilayer MoS₂ [40] and interlayer conductivity of grapheme [41,42]. At low interlayer twist angles, the Moiré superlattice generates a quasiperiodic electronic potential landscape [15], leading to long-range ordering and introducing unconventional quantum mechanical phenomena. For example, small interlayer twist angles in bilayer graphene lead to Hofstadter states [43] and superconductivity [44], while small twists in heterostructures lead to interlayer excitons [45-47]. Understanding and tailoring the electronic states in emerging 2D materials and from Moiré superlattices is currently one of the most exciting areas in solid state physics.

Most of the electronic and quantum states in both monolayer 2D materials and heterostructures are highly sensitive to strain and interlayer structure, and thus may be tuned mechanically. Meanwhile, the ability to deform 2D materials out of plane leads to spatially inhomogeneous strains at the same scale as the mean free path of electrons. Outlined in Fig. 1, these capabilities lead to tantalizing new possibilities for using mechanics to sense, tune, tailor or even reconfigure electronic devices and quantum states. Finally, the same mechanics that allows the fabrication of 2D heterostructures also enables a variety of new fabrication techniques which permit the material to be integrated into new morphologies in ways that are challenging for other material classes. Transferring 2D materials onto arbitrary substrates enables many new ways to induce or sense deformations. Examples include: holes for suspending the 2D materials as membranes, pre-defined 3D morphologies, soft substrates enabling compression, and hinges in free-floating origami

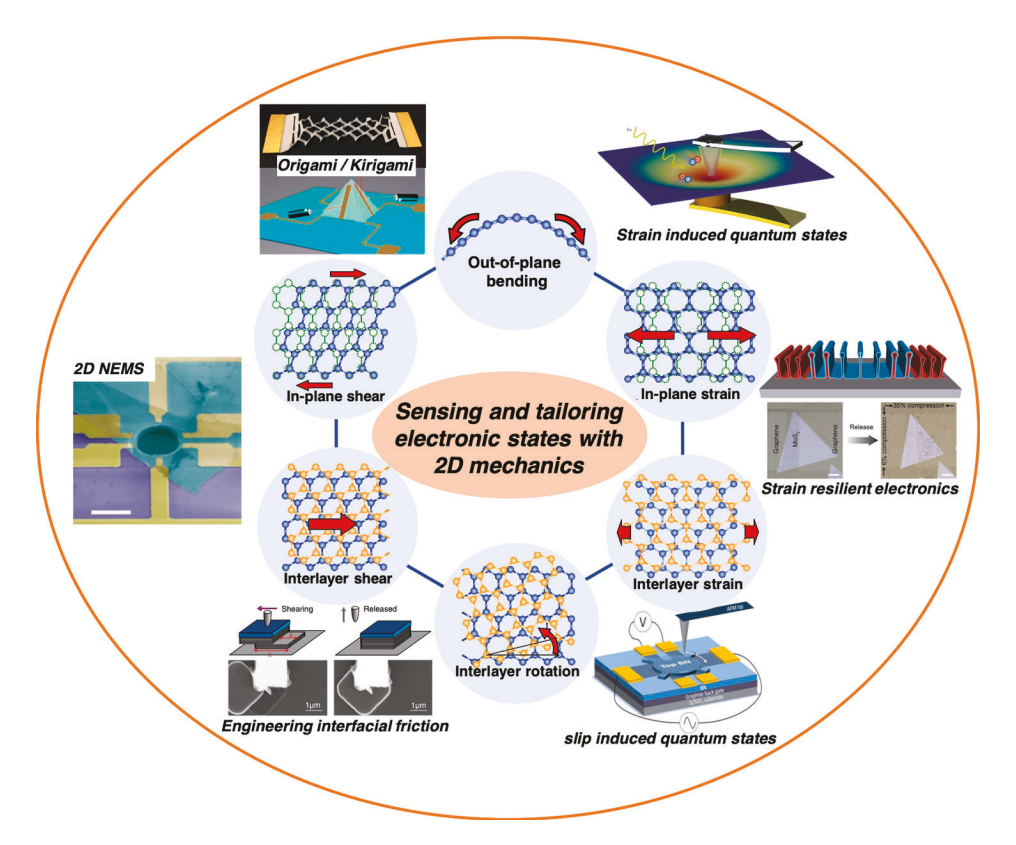


Fig. 1. Possible mechanical deformations in 2D materials and corresponding applications utilizing mechanics of 2D materials. Overview figure includes graphics from [19–25]

or kirigami nanomachines.

In the following sections, we will review how to leverage new fabrication technique to induce different kinds of deformations on 2D materials, the fundamental interactions between mechanics and electronics under each kind of mechanical deformation. We will then connect these interactions to the frontiers of technological applications, new classes of quantum materials, and emerging fundamental scientific investigations.

3. Mechanical sensing with 2D materials

3.1. 2D Nanoelectromechanical systems

Microelectromechanical systems (MEMS) are a diverse, ubiquitous technology in smart electronics and sensing; by extension, nanoelectromechanical systems (NEMS) are orders of magnitude smaller, more deformable, more sensitive, faster, more tunable, and require lower consumption of power. 2D materials are the logical limit of this size scaling, making them naturally ultrasensitive to perturbations in their environment. Moreover, because they are electrically active, many 2D materials are capable of self-sensing their own motion through changes in capacitance or transconductance [48]. A typical 2D mechanical resonator is shown in Fig. 2a. The 2D membrane is suspended over pre-defined trenches or holes and electrically contacted with a source and drain. A global or local gate at the bottom of the trench simultaneously tunes the density of states in the material and electrostatically pulls the membrane towards the gate. Applying a static gate voltage tunes the membrane tension, while applying an radio-frequency (RF) voltage at the right frequency drives the membrane into resonance. The motion is then detected either optically via a change in interferometric conditions or electrically via a change in device conductance resulting from the capacitive tuning of the density of states [48,49]. Fig. 2b shows a typical electrostatic frequency tuning curve [48]. The

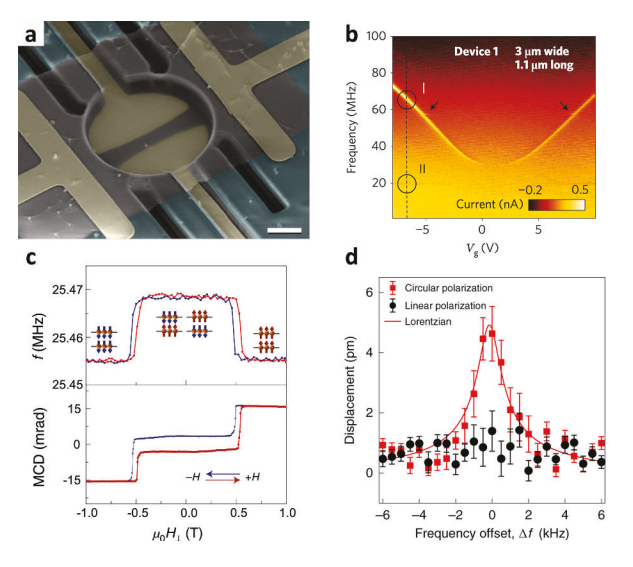


Fig. 2. 2D material based resonators and their characteristics and applications. (a) False colored scanning electron microscopy (SEM) image of suspended monolayer graphene membrane over a hole with two electrodes (source and drain) and a local gate [55] Scale bar = 2 μm . (b) Monolayer graphene tuning curve: 2D map of amplitude versus frequency and gate voltage obtained from monolayer grapheme [48] Large frequency tunability (>100%) is one of the key advantages in 2D NEMS. (c) Resonant frequency (top) and magnetic circular dichroism (MCD) (bottom) vs applied magnetic field in a bilayer CrI $_3$ resonator [56]. (d) Displacement versus frequency obtained from a MoS $_2$ resonator actuated with circularly polarized light (Red) and linearly polarized light (Black), while in a magnetic field [57]. Only circularly polarized light actuates the mechanical motion in the MoS $_2$ resonator, due to a valley overpopulation resulting in a net magnetic moment.

plot shows the frequency versus gate voltage, while the color scale shows the heterodyne current through the membrane, representing amplitude of the motion. These resonators display many properties useful for NEMS. The high Young's modulus and low mass lead to resonance frequencies ranging from MHz [49] to GHz [50]. Yet the high aspect ratio leads to a low out-of-plane bending stiffness and thus large electrostatic [48] and thermomechanical [51] frequency tunability of \approx 10% in RF MEMS [52]. Finally, 2D NEMS display up to 110 dB dynamic ranges of linear operation [53,54], comparable to state of the art MEMS.

2D NEMS serve as a testbed for understanding mechanics at the nanoscale and probing material properties: investigating scaling laws with thickness or lateral dimensions [58–60]; understanding basic resonance properties like frequency [49,59,61], damping [62,63], eigenmode shape [19,64–66] and dynamic range [48,53]; and exploring the relative mechanics of different 2D materials [19,59,60,67–70]. A common challenge to making these studies meaningful is to ensure control over the tension and membrane morphology of atomic membranes, as even small anisotropy strongly affects the resulting eigenmodes and predictability of the structures [61,64].

There is a great deal of interest in leveraging the improvements in tunability, dynamic range, and sensitivity resulting from the low mass of 2D materials to improve existing MEMS and NEMS technologies. Examples in the realm of transducers include demonstrating graphene nanomechanical switches [71], tunable RF oscillators [72], and flat frequency response speakers [73-76]. Perhaps the most intriguing feature of 2D NEMS is the high sensitivity to perturbation, which is ideal for highly responsive sensors [77]. For example, graphene resonators report force sensitivities of 390 zNHz^{-1/2} [78], which is comparable to state of the art force sensitivities of 510 zNHz^{-1/2} in microscale resonators [79]. Implementations include mass/chemical sensors [48,80], accelerometers [81], and bolometers [82]. In most cases, all of these applications operate on similar principles as their larger scale cousins and are at least comparable to the state of the art. However, it is unlikely that we will be replacing any traditional MEMS technologies with 2D materials anytime soon for the same reasons that we will not soon be replacing silicon transistors. In most cases, sensor technologies demand easy calibration and reliable, reproducible operation. Because even small inhomogeneities lead to drastic changes in tension and frequency, the improvements in sensitivity and tunability of 2D resonators do not overcome the challenges in reproducibility and reliability. A more promising route is to focus on what makes 2D materials unique, or in applications where variability is less important.

3.2. Frontiers in 2D NEMS

Looking forward, there are two promising thrusts in 2D NEMS.

The first thrust involves turning the ultra-high sensitivity of 2D devices back upon themselves to directly probe the material properties of the 2D membrane. Examples include probing the structure of van der Waals interfaces [68,69,83], in-plane material properties like the thermal conductance [84,85], phase transitions [86,87], or changes in electronic or quantum states [88,89]. There are two different categories in this frontier. First, any change in structure, whether it is from the dynamics of an interlayer solitons [69,83], thermal expansion [84,85], or a change in phase of the materials [87], will lead to a detectable change in strain in the resonator. Second, a change in electronic structure will lead to a change in response to external forces. Early examples include measuring the Landau levels in graphene resonators under magnetic fields [88,89] and measuring the emergence of a charge density wave phase in a NbSe2 resonator [86]. More recent examples include mechanically probing ordering in 2D magnets [56,87] and the valley overpopulation in transition metal dichalcogenides [57]. Fig. 2c (top) shows the resonant frequency of a bilayer CrI3 resonator as a function of external magnetic field applied perpendicularly [56]. The

discrete jumps are a result of the change in the strain level on the membrane due to the anti-ferromagnetic to ferromagnetic phase transition. The bottom in Fig. 2c shows the magnetic circular dichroism measurement of the resonator. The spin-flip transitions are evident from the graph, located at the same magnetic field values where the frequency jumps occur. Another example shown in Fig. 2d shows the mechanical response in a MoS₂ resonator when exciting one valley state with circularly polarized light that induces a net magnetic moment [57]. By applying a vertical magnetic field gradient to the sample, a periodic modulation of the valley population induces a periodic dirving force in the membrane. More generally, mechanics is a flexible probe to study the many electronic states and phase transitions not only in 2D but also complex ultrathin 3D materials [90].

The second thrust involves understanding and leveraging the strong connections between nonlinear dynamics, entropic mechanics, and dissipation in 2D NEMS at low and high temperature. 2D NEMS display strong nonlinear phenomena, which are useful in signal transduction and enhancing sensitivity. Examples include nonlinear coupling between modes [55,63,91], parametric amplification and cooling [92,93], and stochastic switching between bistable states [94]. Among the demonstrated applications of nonlinearity are the dynamic determination of Young's modulus [95] as well as the enhancement of mass [96,97] and force sensing capabilities [98].

However, the combination of low mass and ultra-high aspect ratio means that 2D material resonators have both a high amplitude response to even very small forces and a low onset of nonlinear motion. At room temperature, the high responsivity results in large ~1-10 nm thermal fluctuations, large enough to not just perturb, but dominate the effective tension, spring constant and dissipation [95,99,100]. In this regard, the graphene resonator behaves more like an entropic spring than continuum membrane, leading to non-intuitive behavior [101]. For example, at low temperature, the quality factor of 2D resonators is very high in the range of $^{\sim}10^4 - 10^6$ [48,61,67,102,103]. In contrast, at room temperature, thermal fluctuations lead to dynamic changes in membrane tension, causing the quality factor to drop to ~10-100, an order of magnitude lower than most silicon MEMS [48,49,61]. Since entropic springs do not obey continuum mechanics, e.g. that the properties will depend linearly on device dimensions, they make it tricky to directly measure continuum properties which are related to stress and strain, like thermal expansion coefficient or Young's modulus [104]. Since the quality factor determines the ultimate sensitivity, and efficiency of numerous MEMS/NEMS technologies, while predictable continuum properties directly affect reliability and reproducible device behavior, understanding and ultimately gaining control of nonlinear thermal fluctuations is critical [105].

Looking to the future, one particularly interesting direction would be to leverage the thermal fluctuations to enhance optomechanical heating and cooling of the resonator for quantum information. For example, graphene resonators display strong optomechanical coupling at room temperature, and show heating or cooling depending on the light gradient [106]. Since the low quality factor at room temperature is primarily determined by thermal fluctuations it should be possible to not just cool the resonator, but correspondingly dramatically tune the effective quality factor and damping. Theoretically, the combination of high frequency, low spring constant and high Q of 2D resonators at low temperature make them ideal candidates for using optomechanics to help cool resonators close to the quantum ground state of motion, with applications in quantum information. The high frequency of 2D resonators of up to 1 GHz mean they will reach the quantum limit of motion at accessible temperatures. Simultaneously, at low temperature, the combination of the low spring constant and high Q of 2D resonators results in a large and easily-detectable amplitude of motion of >1 pm, even at the quantum limit.

4. Mechanically reconfiguring 2D materials

Because of their ability to withstand large deformations without fracture, 2D materials are an ideal candidate for strain engineering to manipulate the electronic structure within the material, and straintronics for engineering systems in which deformations play a key role in tailoring their behavior. In reverse, the ability to curve out-of-plane via crumpling or patterned origami folds enables 2D materials to minimize or control strain transfer even under very large substrate deformations. In either case, the interaction of the 2D membrane with the substrate and interfacial mechanics plays a key role in determining the magnitude and kinds of deformations that may be induced.

4.1. Behavior of 2D materials under strain

As with any material, the photonic and electronic properties of 2D materials are highly sensitive to strain. One advantage of 2D materials is that they are stable as freestanding membranes, and thus do not solely rely on techniques like epitaxial growth to induce strain [107,108]. Instead, uniaxial or biaxial strain is induced through a variety of techniques, including: transferring 2D materials onto prepatterned surfaces [109–111], through nanoindentation [112,113] or gas pressure induced bulge testing [114,115], thermal expansion differentials [116–118], hydrostatic pressure [57,119,120], 2D membranes on soft substrates under bending and stretching [121–129]. In the discussion below, we will focus primarily on studies on soft substrates, but the lessons learned may be extracted from, and are relevant to the other approaches.

One of the simplest approaches to strain engineering in 2D materials is to transfer the monolayers or few layers onto deformable substrates like polydimethylsiloxane (PDMS), then bending or stretching the substrate, which causes a uniform uniaxial strain on the 2D material on the surface [121-128]. In all cases, the mechanics of the van der Waals interface between the 2D material and the substrate is critical. Typically, because the in-plane Young's modulus is large compared with the van der Waals forces, the strain limits are determined not by the mechanics of the 2D material, but by the limits of friction or adhesion of the membrane on the surface, as well as localized substrate shear under the membrane [130]. Slip at the van der Waals interface relieves the strain accumulation in the 2D materials for both tensile [125,131,132] and compressive strain [133]. Therefore, the induced accumulated strain on the 2D membrane is only limited to 1–2%. These limits may be overcome by additional anchoring, for example by polymer encapsulation of the 2D material [134], or by depending on adhesion rather than friction in bulge testing [114,115,135] which may achieve strains of up to 6%.

The change in orbital overlap coming from strain tunes the phononic and electronic properties of 2D materials [121]. Fig. 3a plots the position of Raman active phonon modes versus strain. The plot reveal that introducing uniaxial in-plane tensile strain in monolayer graphene splits the Raman G peak into G⁺ and G⁻ subbands which redshift at a rate of 10.8 cm⁻¹/% and 31.7 cm⁻¹/% respectively, while the 2D peak redshifts at a rate of 64 cm⁻¹/% [122]. Similarly, strain also tunes the band structure of semiconducting 2D materials [125,126,128,129,135]. Fig. 3b shows the tuning of the direct and indirect exciton transition energies in monolayer WS2 as a function of tensile strain [136]. The optical band gap of monolayer MoS2 decreases linearly at a rate of about 45 meV/% with increasing tensile strain, and there is a crossover from direct band gap to indirect bandgap at around 1–2% [125]. The bandgap tuning also directly affects the responsivity of 2D devices. For example, Fig. 3c shows the photoresponsivity versus wavelength of a MoS₂ based photodetector while varying the tensile strain in the 2D membrane. The inset shows the dynamic time response. The photoresponsivity increases by 2 orders of magnitude when the strain varies from 0.8% to 0.48% [129].

Another versatile method for controllable deformation in 2D materials is to suspend 2D membranes over sealed microchambers and use a differential gas pressure to effectively blow the membrane up like a

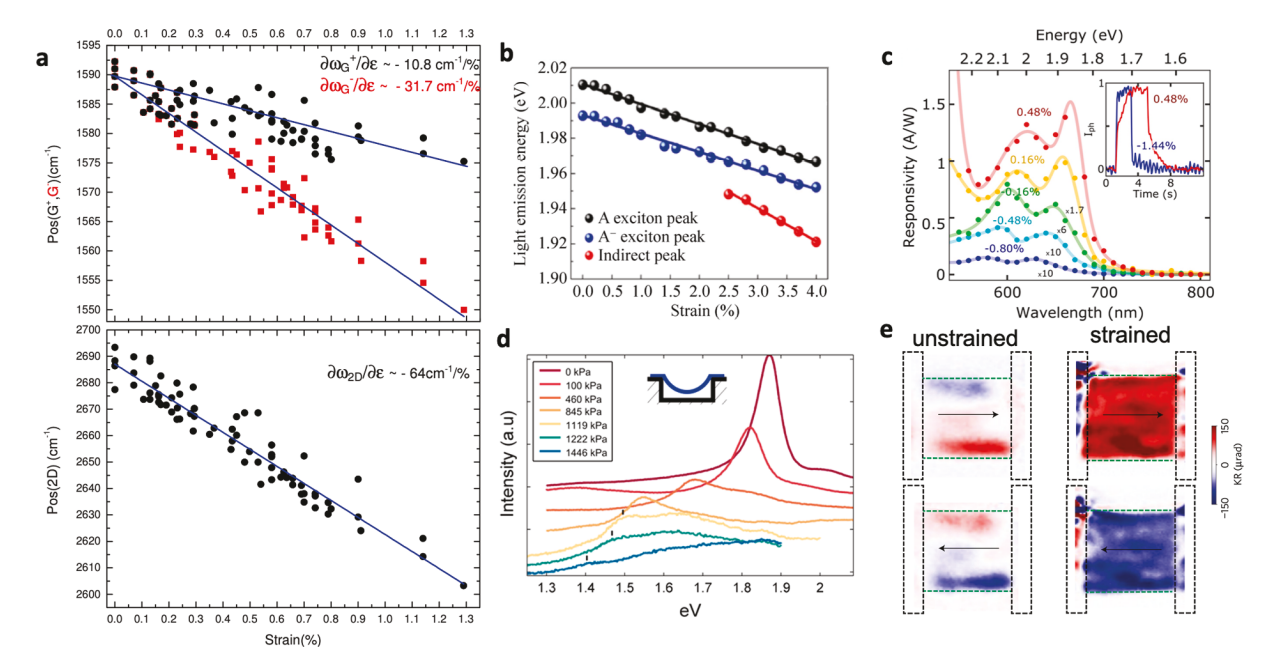


Fig. 3. Tuning optoelectronic and magnetic properties of 2D materials. (a) Raman peak shift of the G⁺ and G⁻ (top) and 2D peaks of monolayer graphene as a function of applied uniaxial strain [122]. (b) Photoluminescence exciton energies of A, A₋, and I peaks for CVD monolayer WS₂ as a function of uniaxial strain [136]. (c) tunable cut-off wavelength photodetector by modulating strain on monolayer MoS₂ [129]. (d) Photoluminescence spectra for monolayer MoS₂ suspended over a sealed microchamber using differential gas pressure to induce biaxial strain of up to 5% [135]. (e) Kerr rotation image of unstrained (left column)) and strained (right column) single layer MoS₂ device under opposite bias (black arrow) [137].

balloon [135,138], similar to bulge testing commonly used in mechanics measurements of macro scale membranes. The bulge testing was originally used to demonstrate that monolayer graphene is effectively impermeable to gases [138], though recently evidence of graphene membranes on graphite microchambers shows that the impermeability does not extend to atomic hydrogen [139]. The magnitude of bulge and shape of the inflated membrane provides a great deal of information about the mechanics of the membrane. Measuring the delamination of the 2D membrane from the edge of the cavity allows extraction of the 2D membrane to surface [114,115]. For example, the adhesion energy of monolayer graphene is $0.45 \, \text{J/m}^2$, nearly 50% larger than the $0.31 \, \text{J/m}^2$ adhesion of 2–5 layer graphene on the same surface. This difference is due to the liquid-like conformation of monolayer graphene to the rough SiO₂, a direct result of the much lower monolayer bending modulus compared with few layer graphene.

The bulge test is also used to tune the strain of 2D materials. Fig. 3d shows the tuning of the optical band transition of a free-standing MoS₂ membrane under pressure induced biaxial strains of up to 5.6%. Using similar techniques to measure the thermal conductivity of strained graphene by tracking the evolution in the Raman spectra reveals that the thermal conductivity drops 20% when 0.12% biaxial tensile strain is applied [140]. Applying the same principle to multilayer 2D membranes, the 3D bulge may effectively induce an interlayer shear. For example, measuring the Raman G-peak shift in bulged bilayer graphene showed that the interfacial shear stress at the van der Waals interfaces of between graphene layers was 40 kPa, much lower than the 1.64 MPa shear stress between graphene and SiO₂ substrate [141]. Similarly, the evolution in the bulge shape of 2D multilayer membranes under varying pressure revealed that interlayer slip was lowering the effective bending modulus at larger deflections [142].

In addition to simple bandgap tuning, strain may also be used to tune the quantum properties and phases of 2D materials. For example, Fig. 3e shows maps of the Kerr rotation of polarized light reflected off a $\rm MoS_2$ phototransistor while varying the sign of the in-plane bias (top versus bottom images), and under no strain or 1% strain applied along the x-axis (left versus right images). The measurement is taken using magneto-optical Kerr effect (MOKE), and the color scale represents the net

magnetization. The maps reveal a valley hall effect in the unstrained material and a uniform and electrically controlled magnetization in the strained material. The net magnetization in the strained sample is due to uniaxial in-plane strain breaking the 3-fold symmetry of the monolayer MoS₂ lattice, and thus breaking the degeneracy of the spin-orbit coupling in the valleys resulting in a valley magneto-electric effect [137]. As another example, at high enough strains, it becomes possible to induce dynamic phase transition between the semiconducting 2H and metallic 1T' phases. Theoretical calculations predict that very high equibiaxial strain of 10-15% is necessary for the transition to metallic phase for most members of the TMDC family. The exception is MoTe₂ which transforms into the metallic phase with a tensile strain <1.5%, and WTe2 which is naturally in the 1T' phase at zero strain [143,144]. Consequently, alloyed Mo_xW_{1-x}Te₂ is close to the phase transition at equilibrium, enabling non-volatile switches by externally inducing the phase transition with gates and strain [143,145–147].

The examples above are for in-plane strains. However, applying out-of-plane strain via hydrostatic pressure is an alternate method for mechanical tuning of quantum properties. Applying pressure on 2D heterostructures or multilayers alters the interlayer spacing, and thus the coupling between the layers. For example, while superconductivity normally can only exist at very precise magic angles in twisted bilayer graphene, applying hydrostatic pressure of $^{\sim}2.5$ GPa broadens the range of angles where flat band states [148,149] may exist, and may be used to induce superconductivity [119]. Similarly, in magnetic 2D materials like CrI_3 , hydrostatic pressure tunes the interlayer spacing and the ferromagnetic or anti-ferromagnetic ordering of multilayer stacks [57,120].

Looking forward, there are still many other materials and properties that may be tuned with uniform strains. However, a very interesting research direction will be to integrate tuning quantum states with the more advanced 3D deformations discussed in the frontiers below to gain spatial control, device integration, and reconfigurability.

4.2. Frontier 1: Engineering quantum systems through three-dimensional deformation

One frontier of research is to leverage inhomogenous strain brought

on by 3D deformations in 2D materials to induce new control over electronic states. Because of their low bending stiffness [10,142], in most cases 2D materials energetically favor out-of-plane deformations when subjected to in-plane stress. Engineering 3D deformations at different length scales induces local strain gradients or periodic modulations of the strain. As discussed in the previous section, strain directly modulates the local band structure of the material, so spatially inhomogeneous strain leads to spatial modulations of the band structure, both work function and band gap. These variations are analogous to to what is normally achieved through heterostructures of different materials like one finds in solar cells, light emission devices, and quantum wells which are commonly used to trap or direct the flow of charge. Thus the strain gradient induced local variations generate local electric fields which direct the flow of excitons. Similarly, points of high strain or curvature, and corresponding smaller bandgap lead to exciton concentration [109], strain tuned single quantum emitters or artificial atoms [110,111,113], or pseudomagnetic fields [150]. Periodic strain superlattices lead to zone folding and new quantum states [17], similar to what is often achieved with twistronics.

Fig. 4a-b shows one strategy to achieve local strain gradients in a 2D membrane by transferring the membrane onto a nanoscale patterned substrate [109]. Similar results have been demonstrated using other strategies like nanoindentation [113], localized wrinkling [60,151], and on nanobubbles [152,153]. Fig. 4a shows a SEM image of MoS2 monolayer on the corrugated substrate, while Fig. 4b shows corresponding profile and the spatially modulated quasiparticle energy gap of the MoS2 [109]. When a 2D material is transferred onto a 3D topology, a combination of surface tension drying dynamics during transfer and the van der Waals adhesion between the membrane and substrate pulls the membrane down to conform to 3D topologies. The perturbation from the natural flat state of the 2D material leads to inhomogenous strains. Typically, the tensile strain is maximized at points of high curvature, like the tips of the cones, leading to points of smaller quasiparticle bandgap only a few nanometers in size [109]. The strain gradient away from the cone causes a continuously changing quasiparticle bandgap. Similar results may be achieved via nanoindentation with an AFM tip [154,155], transferring onto nanopillars [110,111], and indenting and

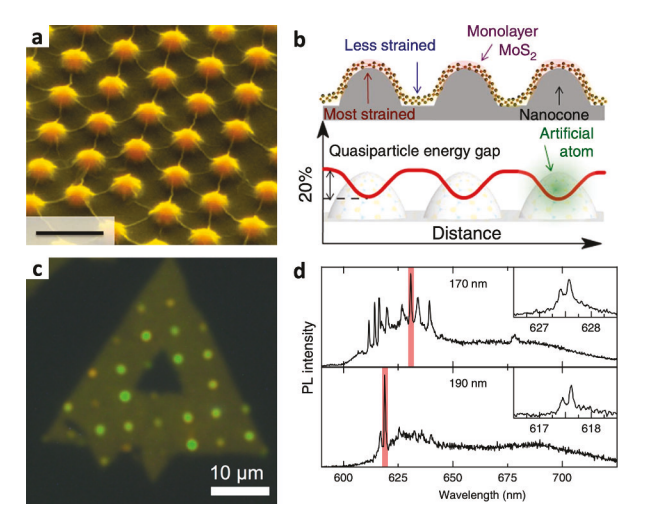


Fig. 4. Method of inducing tensile strains and strain engineered optoelectronic devices. (a) False-colored scanning electron microscopy (SEM) image of the MoS_2 on top of nanocones. Scale bar is 500 nm. (b) Schematic of MoS_2 on the SiO_2 nanocones, and corresponding band gap of SiO_2 . Presence of nanocones induces tensile strains on SiO_2 , which modulates the band gap spatially [109]. (c) Fluorescence image of SiO_2 monolayer after a grid of atomic force microscopy (AFM) indents were introduced [113]. (d) Photoluminescence (PL) spectra of 1L-WS2 at 10 K, on top of nanopillers pillars of 170 nm (top panel), and 190 nm (bottom panel) height. Insets are high-resolution PL spectra of the red-highlighted spectral regions, where the single photon is emitted [110].

changing the shape of the 2D material on a plastically deformable substrate [113]. For example, Fig. 4c shows fluorescence maps of a CVD grown monolayer WSe₂ crystal with periodic indentations on a thin film of PMMA [113]. The strong enhancement of the luminescence at the indentation points is a result of exciton diffusion from the regions of low strain to the points of high strain. It is important to note that a simple change in PL intensity is not sufficient evidence to uniquely identify exciton diffusion, as changes in interferometry, changes in dielectric environment, changes in doping may all also contribute. For example, recent results on AFM indented WS₂ suggest that some fraction of the signal change is due to neutral to charged exciton conversion [154]. Unraveling the relative contributions from these different effects for different materials and strain paradigms is an important future direction.

In addition to the bandgap tuning, like the behavior shown in Fig. 4b, high strains at the apex of pillars [110] or on nanobubbles [156] may be used to isolate single quantum emitters. For example, Fig. 4d shows the low temperature (10 K) PL spectra at the apex of two pillars different heights [110]. Sharp optical transitions become visible in the broader spectra and these transitions appear to be tunable with strain. These features are difficult to uniquely identify or control, so whether they are a result of strain induced artificial atoms or the strain tuning of defects within the crystal lattice is still under debate.

Another property that rises from localized strain and curvature is the introduction of strong pseudomagnetic fields. For example, the apex of graphene nanobubbles display tuning similar to pseudomagnetic fields of up to 300 Tesla [150]. The combination of electronic and magnetic tuning on curved and strained surfaces also presents a new possibility to induce new quantum states though periodic deformations with sizes below the mean free path of electrons. For example, transferring graphene onto close packed arrays of nanoparticles with diameters 10–100 nm leads to periodic modulations in strain and curvature [157]. The periodic modulations induce electronic superlattices, with secondary Dirac points visible in the electronic transport. Recent predictions and measurements suggest that strain superlattices at just the right size scales will lead to flat band states similar to those induced by Moiré superlattices [158]. Taken together inhomogeneous strain whether from strain gradients, points of high strain, or superlattices provide a new knob for engineering many different quantum phenomena in 2D materials and heterostructures, and we are only now gaining the control to deterministically manipulate these systems.

4.3. Frontier 2: Tailoring strain transfer and 3D morphology of 2D membranes on soft substrates

There is some ambiguity in the literature—are 2D materials highly strain resilient, or are they highly tunable with strain? Both possibilities are useful, leading to either strain resilient electronics or mechanically reconfigurable quantum materials. Summarized in Fig. 5, the incongruity rises from how strain is being transferred into the material and what kinds of deformations are present. Fig. 5a-b shows scanning electron microscopy images of 3D patterns generated in a graphene sheet under mechanical deformation: the graphene delaminates and buckles under uniaxial compression and crumples under biaxial compression respectively [159]. On the other hand, Fig. 5c shows much more regular and longer scale wrinkles from a 2D material supported by a 15 nm thick ALD Al₂O₃ film while being uniaxially compressed by 10% on a soft substrate [151]. These differences in morphology rise directly from mechanical instabilities of thin films under compression on a soft substrate, often called Ruga [160], and lead to distinctly different behavior. Without any support, the adhesion and friction energy of monolayer 2D materials on a surface is weak compared with the mechanical moduli, so the interfacial energies dominate the mechanics. As a result, monolayer materials on a prestretched substrate easily delaminate or slip over the surface to relieve the compression as the substrate is released [133], leading to complex 3D crumples and folds [133,159,161-163]. In

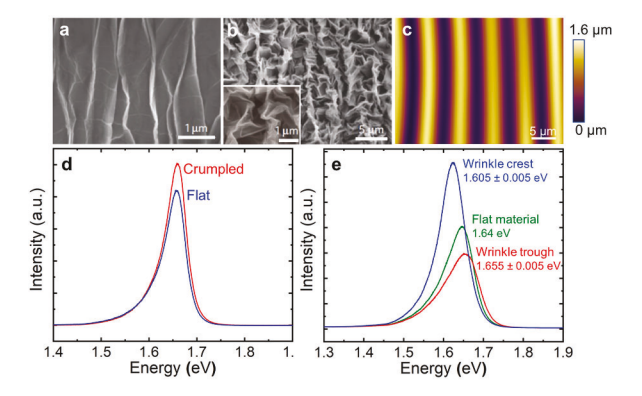


Fig. 5. Comparison of crumpling and wrinkling. (a-b) Scanning electron microscopy (SEM) images of compression induced deformations on a monolayer graphene sheet on a soft substrate: (a) delaminated buckles under uniaxial compression [159] and (b) crumples under biaxial compression [159]. (c) Atomic force microscopy (AFM) image of wrinkled WSe₂ laminated onto 15 nm Al₂O₃ on very high bonding tape (VHB) under 10% uniaxial compression [151]. (d-e) Photoluminescence (PL) spectroscopy of flat and crumpled WSe₂ under 15% biaxial compression [20] (d), and Wrinkled WSe₂ under 10% uniaxial compression [151] (e) showing the effect of the morphological change on the optical property of the material.

contrast, if the monolayer is anchored via strong adhesion to another layer, e.g. either a chemically-modified skin layer on the substrate [164], a polymer top layer [134], a thick multilayer material [165], or an ALD grown film [151], the additional layer both stiffens the film and prevents delamination or slip. The supporting layer leads to a more periodic uniform wrinkling with a much longer wavelength. The larger deformations, and suppression of slip in the 2D monolayer, leads to stronger tuning of the in-plane strain. Fig. 5d-e visualize this difference, comparing the photoluminescence spectra of monolayer WSe2 samples that have been biaxially crumpled by 15% and uniaxially wrinkled by 10% respectively. Crumpling shows no significant shift of the bandgap (~2 meV) compared with the flat sample, leading to <0.05% average strain in the 2D material [20], while the wrinkled sample shows downshifting and up-shifting of the bandgap on the crest and trough of the wrinkles, corresponding with tensile and compressive strains of ~0.5% [151]. Similar bandgap tuning is observed in wrinkled WS₂ samples corresponding to a local strain of 0.83–1.33% [165]. These results show that controlling the interfacial interactions and stiffness is key to controlling the morphology and size scale of the 3D deformations, which in turn is directly relevant to technologies based on 2D materials. The larger wrinkled morphologies where strain is allowed to build up are directly relevant to mechanically reconfiguring strain and strain gradients, which gives a new knob to tune the 3D deformations discussed in the previous section. The next steps will be to integrate electrodes into the large scale wrinkles to form strained devices where it is possible to simultaneously electrically interrogate or manipulate the strain-induced quantum states.

In contrast, in crumpled systems the feature sizes of the folds are much smaller, around the 10–100 nm size scale [159]. While the out-of-plane 3D deformations are large compared with the material thicknesses, the energy of bending is so small that they prevent the average in-plane strain from building up. As a result, the crumpled 2D membranes offer mechanical stability, allowing reversible substrate stretching of up to 300–400% without fracture [159,166–168], far larger than the $^{\sim}20\%$ fracture strain of a flat 2D material [7]. This difference is analogous to the relative stretchability of a crumpled versus flat sheet of paper.

In addition to the stretchability, one of the great advantages of the crumpled morphology is the dynamic tunability of the material morphology, which directly affects material properties. Fig. 6a-b shows that through simple modifications, it is possible to engineer highly

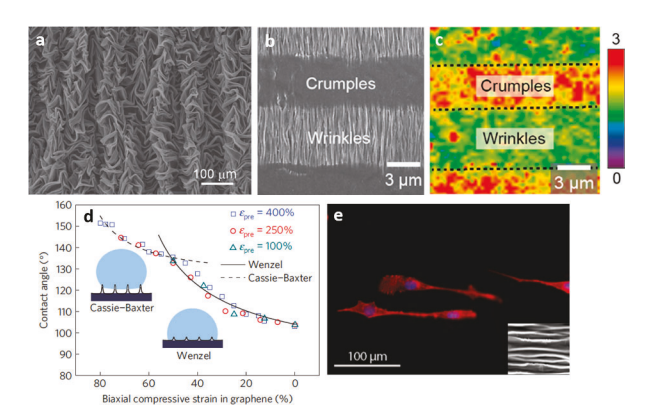


Fig. 6. Controlled crumpling and wrinkling of graphene sheet generates novel surface properties. (a) Scanning electron microscopy (SEM) image of biaxially crumpled patterns generated in a graphene paper [166]. (b-c) Area selective surface chemistry in deformed graphene. SEM image of multiscale uniaxial wrinkles and crumples in graphene (b) and corresponding selective fluorination of graphene showing the variation in $\rm I_{G}/\rm I_{2D}$ peak intensity ratio [169]. (d) Water contact angle as a function of biaxial compressive strain in grapheme [159]. (e) Fibroblast culture on wrinkled graphene showing highly aligned cells. Fluorescence image of Actinphalloidin (red) and nuclei (blue) for NIH-3T3 and NHF cells cultured on 200 nm wrinkled s-GO substrate (~25 μm period) [170].

complex and disordered multiscale 3D features. In Fig. 6a complexity rises through multiple stages of compression [166], while in Fig. 6b the complexity rises through spatially modifying the substrate surface chemistry [169].

The high surface area and nanoscale features make these crumpled 2D materials useful for applications as multifunctional surfaces [159,169–172]. For example, Fig. 6b-c shows a side by side SEM and a Raman map of the same region of crumpled/wrinkled graphene which has undergone fluorination. The graphene I_G/I_{2D} Raman peak ratio varied between the wrinkled and crumpled regions due to the variation in fluorine adsorption coverage [169], showing that the surface chemical reactivity of the graphene can be tuned by the morphology. In a second example, Fig. 6d compares the water contact angle on crumpled graphene as a function of biaxial compressive strain [159]. The contact angle increases from 100° to 150° as the biaxial strain in graphene is tuned from flat 0% to highly crumpled 80%. Crumpling by varying the substrate compression modulates surface wettability, with rougher surfaces leading to larger hydrophobicity. In a third example, in mechanobiology, surface structure is often used to direct and template the growth of cells. Fig. 6e shows a fluorescence image of fibroblast cells cultured on uniaxially crumpled graphene, where the cells align along the folds [170]. Finally, multifunctional surface properties may be further tuned through the integration of lower dimensional structures such as nanoparticles and nanowires into the crumpled membranes, leading to new device architectures and functionalities such as nanoplasmonic sensors [173-175]. Taken together, tuning the interfacial interactions between the 2D material and the soft substrate makes it possible control the mechanically driven surface instabilities resulting in either strain-dependent quantum states, or highly-stretchable multifunctional surfaces and devices.

4.4. Frontier 3: Strain resilient electronics

One of the first applications proposed for graphene was as a transparent and conductive electrode [176,177] or flexible field effect transistor [178–183]. However, to bring the true versatility of 2D materials to deformable electronics, it is necessary to combine two innovations: heterostructures and crumpling.

First, incorporating heterostructures from 2D materials onto soft substrates enables the fabrication of fully functional flexible electronics

[37,183–185]. For example, one demonstration showed a bendable, fully functioning transistor comprised of all 2D materials on a flexible substrate, with an MoS_2 channel, h-BN dielectric and graphene gate electrode [37]. The transistor demonstrated high mobility of 29 cm²/Vs which remained unchanged under tensile strain of up to 1.5%. Another demonstration showed flexible graphene microwave transistors for lownoise analog amplifiers and frequency mixers useful in wireless communications. In such applications, the applied tensile strain shifts the effective charge neutrality point [178,186] of the transistor.

Second, wearable electronics require devices and materials capable of undergoing not just bending, but stretching [187]. Utilizing the concepts of crumpling discussed in the previous section, there have been many demonstrations of stretchable electronics from crumpled graphene and semiconducting 2D materials. In some cases, the crumpling simply enables stretchability, while in others it drastically enhances the performance of the device. For example, Fig. 7a shows the CV curves of a crumpled graphene supercapacitor under different uniaxial tensile strain levels [166]. The CV curves remain almost unchanged under strain from 0% to 150%, because the effective surface area of the crumpled graphene membrane stays constant. In contrast, Fig. 7b compares the Dirac point shift of a crumpled versus flat graphene field effect DNA sensor as a function of the added target DNA concentration [188]. The crumpled device demonstrates nearly three orders of magnitude more sensitivity than the flat sensor, and is able to selectively detect DNA down to attomolar concentrations. Meanwhile, in monolayer 2D material devices, crumpling tunes the piezoresistivity and photoresponsivity, as observed in crumpled grapheme [167,189], and crumpled ReSe₂ [190]. These studies found that crumpling through biaxial substrate compression of up to 300% lead to significant changes in conductivity of ~50%. At the same time, photoresponsivity changes by up to 10x, mainly due to enhanced absorbtion through the densification of the material [167] (compression of 300% along each direction, leads the same amount of material in about 1/10th the area). However, these changes are actually surprisingly small when compared with strain on flat samples, which display similar changes at 1% strain [129].

Another promising research direction is the ordered folding or cutting of two dimensional membranes, known as origami and kirigami, to generate ordered three-dimensional structures [21,191–194]. The principles of origami and kirigami are scale invariant and only limited by the mechanics of the membrane material, so these approaches offer versatility in design of deformable structures unavailable in the

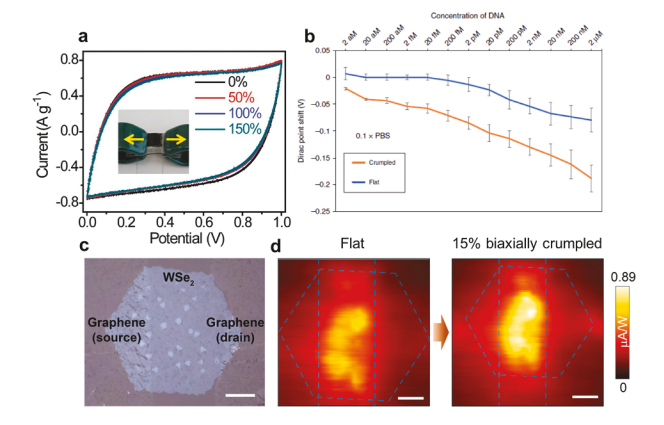


Fig. 7. Devices utilizing novel properties of crumpled 2D materials. (a) The CV curves of a crumpled graphene supercapacitor collected at a scan rate of 10 mVs^{-1} under uniaxial strains of 0%, 50%, 100%, and 150%. The thickness of the graphene paper is 0.8 mm measured at dehydrated state [166]. (b) The Dirac voltage shift of a flat vs. crumpled graphene FET sensor as a function of the added target DNA concentration [188]. (c) Crumpled phototransistor from graphene contacts to a monolayer WSe₂ channel [20]. (d) Scanning photoresponsivity maps of a graphene-WSe₂ phototransistor under flat and 15% biaxially crumpled condition [20]. Scale bar is $10 \text{ }\mu\text{m}$.

disordered crumpled systems. However, these approaches are largely limited to freestanding or delaminated membranes, because the low bending stiffness means the 2D material needs to be decoupled from the surface, or else the substrate interactions will overwhelm the influence of all other forces. For example, patterning kirigami cuts into the graphene enables highly stretchable and ultrasoft freestanding electrodes [21], or MoS₂ photo/temperature sensors [194]. In another example, integrating 2D materials into foldable 3D structures which buckle delaminate from the surface allows the use of graphene as a conductive hinge [195] or MoS₂ based 3D photodetectors [22,196]. Finally, integrating 2D membranes with other chemically or light active materials like polymers or ALD films to create asymmetric bimorphs has promise for introducing externally controllable actuators [191] to build free-floating microbots that can grip cells [197,198] or swim [199].

All of the previous demonstrations are on single 2D materials and still utilize conventional metals or thin films to make contact to the active regions or act as mechanical supports. To take full advantage of the mechanical properties of 2D materials for stretchable electronics, it is necessary to combine the concepts of heterostructures with crumpling. Shown in Fig. 7c, we recently demonstrated all-2D crumpled phototransistors using graphene contacts to a WSe₂ channel [20]. Because of their matched mechanical moduli and low interfacial friction, the graphene contacts maintain conformal interface with the WSe2 channel through the crumpling process. Fig. 7d shows spatially resolved maps of the photoresponse of the device before and after 15% biaxial crumpling. The photoresponse changes by only 20%. This small change can be compared to the factor of 100 change of a flat MoS2 phototransistor under ~1% strain described in Fig. 3c [129]. Taken together, these results, along with the morphology and low bandgap tuning shown in Fig. 5d, show that the crumpling process prevents the buildup of strain, demonstrating the potential for strain resilient electronics.

Looking into the future, there have been an enormous variety of high-performance device demonstrations from 2D heterostructures. By exploring crumpling, wrinkling, origami and kirigami on more complex 2D heterostructure geometries, for example logic devices and sensors, it should be possible to realize high mobility electronics that are also deformable. These devices would have distinct advantages over other stretchable electronics technologies like polymers and or nanomembranes made from conventional materials because they are both high mobility and deformable down to the nanoscale. Moreover, they would also offer potential to integrate electronic elements into the hinges and panels of mobile microbots, vastly enhancing their potential capabilities.

5. Configuring interlayer alignment in 2D heterostructures

In the examples above, most work has focused on single materials, or has treated the layers as electrically independent. Yet, in most cases, the layers interact with each other and the external environment, causing the electronic properties to be sensitive to details like the number of layers and interlayer alignment. These interactions may be manipulated in multilayers and heterostructures by tailoring the interlayer symmetry, stacking, and alignment leading to a new class of quantum materials based on misaligned 2D heterostructures known as Moiré crystals [16,200]. At the same time, the ultralow friction or superlubricity between layers means that even very small perturbations allow the layers to shear or realign, changing the effective interactions. An emerging concept is to apply interlayer strain, twist or shear like to dynamically tune these interfacial properties and engineer mechanically reconfigurable quantum materials and states.

To understand how to manipulate the electronic states, we must first understand the relation between interlayer structure and interfacial friction and adhesion. Long before 2D materials were being used for electronics, they were being used as dry lubricants. The lack of dangling bonds on ultraflat surfaces make van der Waals surfaces a perfect playground for tribology, and understanding the role of crystal lattice on

the origins of friction, stick–slip behavior and superlubricity [201–207]. Studies mainly focused on rubbing macroscale crystals together [208,209], or probing tribology at the nanoscale with scan-probe lateral-force microscopy techniques [202,210–214]. For example, Fig. 8a plots that the effective friction of a graphite probe on a graphite surface as a function of interfacial alignment, measured using a custom lateral force microscope [215]. The friction is relatively large when the layers are aligned (modulo 60° , corresponding with the hexagonal structure of graphene), and is very small when the layers are misaligned. The superlubricity originates from there being no stable equilibrium position when layers become misaligned through twist in heterointerfaces [201], leading to interlayer friction being reduced by 2 orders of magnitude compared with the commensurate multilayers [69,216–219].

Superlubricity enables new methods to manipulate the interlayer alignment at the interface between 2D materials through slip in ways that are not possible with conventional 3D materials. For example, one early demonstration used microprobes to laterally push on microscale pillars or "mesas" patterned onto a bulk crystal of graphite [11,23]. The graphite pillars cleaved at a random interface, at which point the top layers slipped easily off the edge of the pillar while undergoing both shear and rotation. Upon release of the probe, due to the relative competition between twist independent adhesion energy and twist dependent friction, the top layers either spontaneously retracted back or stayed in position. depending on whether they were twisted or remained aligned with the underlying pillar. As another demonstration, shown in Fig. 8b, engineering asymmetric pillars and using programmed motions of an atomic force microscope tip made it possible to programmably rotate pillars to different angles and even move the pillars between different bistable states [12]. Fig. 8c, plots the restorative forces versus mesa radius. These resulted yielded the adhesion energy pulling the flakes back to their original configuration to be 0.227 J/m² and the friction coefficient to be ${}^{\sim}7 \times 10^{-5}$, 3 orders of magnitude smaller than typical Coulomb friction between macroscopic bodies [12]. Similar experiments have also been performed on incommensurate interfaces between 2D heterostructures, such as graphene-hBN [24,116,222,223] and graphene-MoS₂ [224]. For these measurements, a 1 Layer - 100 nm thick flake of one material is transferred onto another then pushed around with a probe. The incommensurate heterointerface has much lower friction than the commensurate interfaces of the top and bottom flakes, so all slip is isolated to one location. Because of the different lattice constants of the two materials, the heterointerface is incommensurate at all angles and always displays superlubricity, with similar friction to the twisted homointerface, allowing free rotation and realignment between the layers.

The simple picture of incommensurability and superlubricity becomes more complex when layers are near alignment. In aligned bilayer graphene, small strains, twist, or shear lead to the introduction of solitons, dislocations, and local strain changes in stacking between layers [13,225,226], which can thermally migrate [13] or be pushed around with scan probe tips [132]. The natural width of these solitons is ~10 nm, corresponding with the energy balance between stacking energy and local strain. At very small twist angles or for small lattice constant difference in aligned heterobilayers, the size of the Moiré superlattices becomes large, sometimes $\,\widetilde{}\,10\text{--}20$ nm, leading to regions which are aligned or misaligned and interfacial interaction energies approaching the bending and stretching of the 2D layers. Fig. 8d shows interlayer alignment sensitive dark field transmisson electron microscopy images of twisted bilayer graphene at 0.1° and 0.4° twist angles [220]. The interlayer interactions lead to local reconstruction through local strain or twist, breaking the incommensurability between the layers [220,227], and leading to structures more like networks of solitons. In this limit, the sliding friction between layers depends on the size of Moiré superlattices in both twisted [228] and heterointerfaces [24].

These reconstructions and changes in interlayer alignment directly impact the electronic states. At the simplest level, coarse interlayer twist leads to band structure tuning and charge transfer by tuning interlayer interactions. In order for states between layers to hybridize, or for charge to easily transfer, there must be an overlap in both real-space and in k-space. For example, there is very little tuning of the direct gap states in twisted bilayer MoS_2 [40] or heterostructures [45-47] unless the layers are close to aligned. This is because the direct gap is located at the offset k-point, which means that the position will be different in each layer at all twist angles, except when close to aligned. In contrast, the indirect gap in twisted bilayer MoS₂ is tuned by more than 100 meV due to a ~10% as a function of twist angle [40]. In this case, the indirect gap changes dramatically because it is located at the zero-momentum Γ point in each layer, which will remain overlapped in k-space at all twist angles. Similarly, the same tuning of band overlap in k-space means that $\,$ twist tunes vertical charge transfer in devices from both twisted graphite-graphite [41,42], between graphene-MoS₂ [224], graphenehBN [229,230], and in graphene-hBN-graphene heterostructures [231]. Typically, the highest conductivity and band tuning occur when layers are near alignment. However, at certain key angles, there are

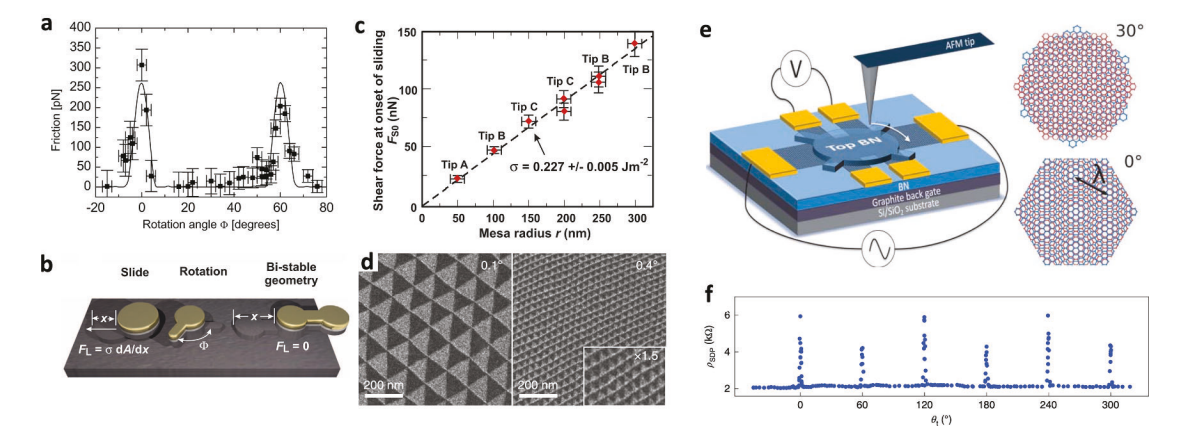


Fig. 8. Design and manipulation of dynamically slippable devices, and measurement of interlayer properties. (a) Friction at the graphite interface as a function of interlayer rotation [215]. (b) Different motions (slide, rotation) of graphite mesa induced by AFM tip manipulation [12]. (c) Adhesion energy at the graphite interface is extracted while measuring shear force of different sized grahite mesa in (b) [12]. (d) Dark-Field Transmission electron microscopy (DF-TEM) of twisted bilayer grapheme [220] at very small twist angles. The contrast is a measure of the relative alignment of layers along a specific crystalographic direction showing where the AB and BA domains are located. The magnitude of reconstruction grows larger at smaller twist angle. (e) Schematic cartoon of the device structure and the experimental technique. h-BN, hexagonal boron nitride, and Moiré superlattice arising between graphene (red) and BN (blue) at different twist angle. (f) Measuring the band structure modification while twisting the angle between graphene and h-BN. Band gap appears in the 60° of rotational symmetry [221].

jumps in the conductivity, corresponding with when higher order bands beyond the unit cell overlap.

5.1. Frontier 4: Reconfigurable quantum materials through interfacial slip in 2D heterostructures

Near alignment there exists a host of interesting phenomena capable of being tuned, and the field is still developing a full understanding of how reconstruction couples to the resulting quantum states. In most cases, the structure is only indirectly controlled via setting the interlayer orientation during the initial stacking to form the heterostructure or due to annealing samples to let them relax into a more favorable energetic equilibrium. At the frontiers of 2D heterostructure research, a more favorable approach would be to use mechanics to program in or reconfigure interlayer alignment. Shown in Fig. 8e, engineering a rotatable h-BN mesa on top of an electrically contacted monolayer graphene field effect transistor enables a scan probe tip to programmably change the twist angle on the h-BN while observing the impact on the intralayer conductivity. Fig. 8f plots the conductivity versus twist, showing that the resistance is constant for most twist angles and spikes up when the layers are aligned to $< 1^{\circ}$ [221]. When the layers are close to aligned, they display secondary Dirac peaks and corresponding Hofstadter effects at low temperature [24].

Looking to the future, we expect to see many of the techniques being applied to tailor the strain and properties in monolayers also applied to heterostructures. Many of the flat band effects and Moiré states seen at low twist should also arise when layers have a low relative strain [158,232]. Recently, reconstruction has been observed on strained heterostructures [233]. However, the vast majority of the techniques involve applying coarse macroscale strains or using scan probes to program in the precise twists. There have been recent innovations using evaporated thin films to induce a relative stress between top and bottom layers [234], as well as the use of gas pressure induced strain on suspended layers [114,115,141]. These techniques add a significant degree of control and programability to the interlayer strain, but are static. We envision that a more favorable approach would be to enable electromechanical tuning of states, discussed in the final section.

6. Future prospects

We have already described useful new technologies and newly enabled fundamental scientific directions in each of the frontiers discussed above. Looking further into the future, we envision the two distinct fields of 2D nanoelectromechanical systems for sensing, and mechanically induced reconfiguring of states to be united to produce devices which use electromechanical forces to transduce and sense quantum states. Doing so will require overcoming challenges in control and reproducibility in constructing 2D devices, but will offer opportunities in enabling some truly unique quantum technologies.

6.1. Challenges

A famous quote from Wolfgang Pauli is "God created the bulk; the surface was invented by the devil". As monolayers with nothing but surface, 2D materials are devilish systems, prone to disorder, and hard to control. Most demonstrations are of hero devices selected from a large set of failed experiments or reporting the results of states which are uncontrolled. The common limitation and underlying challenge for nearly all the frontiers described here is control and reproducibility, and a great deal of effort has gone into mitigating or bypassing these challenges. First there are the challenges common across all 2D materials research: the quality of grown materials [235]; environmental impacts like air sensitivity of some materials [236]. There are the challenges associated with electronics: defining the desired doping [237], contact resistance, and electronic mobility and avoiding inhomogenous doping from the substrate and environment through encapsulation [238]. Then

there are the challenges of scalable manufacturing: scalable synthesis of monolayers with properties rivaling materials exfoliated from bulk [239-241], scalable methods for transfer and producing desired interfacial cleanliness and alignment [242], avoiding processes like metal evaporation which damage surfaces and interfaces [243-245], and atomically precise fabrication methods for accessing one layer but not others within a heterostructure [246]. Finally there are the challenges rising from the mechanical processes. Onset of slip and out of plane buckling or crumpling are nonlinear instabilities which are notoriously sensitive to parameters like the cleanliness of the interface, material quality, surface roughness, and inhomogeneity in strain [133]. Fortunately, many of these challenges are also critical in nearly all applications involving nanomaterials, and realizing nanoscale control is considered a grand challenge by funding agencies and engineering societies. In the meantime, any studies and applications should focus on systems which are robust against variability or allow for variability in their results.

6.2. Future directions: Slippable 2D NEMS

Borrowing the concepts of actuation and transduction from 2D nanoelectromechanical systems and applying them to engineering interlayer strain and slip will enable both a new class of NEMS devices and offer control over a broad class of quantum states. Because of scaling and the aspect ratios of 2D materials, generally electrostatic forces are to weak to generate large enough strains in 2D membranes to significantly alter the band structure. However, because of the much lower energy barrier electrostatic forces may potentially be used to actuate slip between layers and thereby transduce the electronic states. For example, we have recently demonstrated that applying tension to suspended membranes of 2D heterostructures [69] and bilayer grapheme [83] through electrostatic backgates was sufficient to induce interlayer slip and the introduction of soliton defects.

Another example would be to borrow design concepts from MEMS. Conventional MEMS are typically suspended. There have been several proposals of MEMS devices based on laterally actuated heterostructures [247–249], but such structures have yet to be experimentally realized. These proposed device geometries already offer very interesting ideas for new MEMS structures that exploit interlayer slip to produce low dissipation micromotors and switches [250]. Howevever, their design and dynamic behavior also offers a potential for electromechanically reconfigurable interfaces. In these geometries, applied voltages apply lateral forces to heterostructures which, because of superlubricity, will locally slip or strain layers, and thus reversibly reconfigure interlayer alignment while also allowing simultaneous electrical transport measurements to probe the resulting electronic and quantum states.

Taken together, while there are many technical challenges remaining to overcome, there are many opportunities to bring together the diverse fields of straintronics and nanoelectromechanical systems to enable dynamically tunable quantum systems and devices. More generally, utilizing both the unique mechanical and electronic properties of 2D materials offers numerous new directions for both probing and tailoring quantum systems at the forefront of science and technology.

Declaration of Competing Interest

The authors declare that they have no known competing financial interests or personal relationships that could have appeared to influence the work reported in this paper.

Acknowledgements

This research was supported by the National Science Foundation MRSEC program under NSF Award Number DMR-1720633, and the CAREER Award under award number CMMI-1846732. We thank Jangyup Son, Sihan Chen, and Pinshane Huang for helpful discussions.

References

- R. People, et al., Modulation doping in Ge x Si 1-x/Si strained layer heterostructures, Appl. Phys. Lett. 45 (1984) 1231–1233.
- [2] H.M. Manasevit, I.S. Gergis, A.B. Jones, Electron mobility enhancement in epitaxial multilayer Si-Si 1–x Ge x alloy films on (100) Si, Appl. Phys. Lett. 41 (1982) 464–466.
- [3] E.P. O'Reilly, A.R. Adams, Band-structure engineering in strained semiconductor lasers, IEEE J. Quantum Electron. 30 (1994) 366–379.
- [4] S. Manzeli, D. Ovchinnikov, D. Pasquier, O.V. Yazyev, A. Kis, 2D transition metal dichalcogenides, Nature Rev. Mater. 2 (2017) 17033.
- [5] V.K. Sangwan, M.C. Hersam, Electronic Transport in Two-Dimensional Materials (2018).
- [6] S.J. Kim, K. Choi, B. Lee, Y. Kim, B.H. Hong, Materials for flexible, stretchable electronics: graphene and 2D materials, Annu. Rev. Mater. Res. 45 (2015) 63–84.
- [7] D. Akinwande, et al., A review on mechanics and mechanical properties of 2D materials—Graphene and beyond, Extreme Mech. Lett. 13 (2017) 42–77.
- [8] Q. Cao, et al., A review of current development of graphene mechanics, Crystals 8 (2018) 330–357.
- [9] C. Lee, X. Wei, J.W. Kysar, J. Hone, Measurement of the elastic properties and intrinsic strength of monolayer graphene, Science 321 (2008) 385–388.
- [10] E. Han, et al., Ultrasoft slip-mediated bending in few-layer graphene, Nat. Mater. (2019).
- [11] Q. Zheng, et al., Self-retracting motion of graphite microflakes, Phys. Rev. Lett. 100 (2008) 1–4.
- [12] E. Koren, et al., Adhesion and friction in mesoscopic graphite contacts, Science 348 (2015) 679–683.
- [13] J.S. Alden, et al., Strain solitons and topological defects in bilayer graphene, Pro. Nat. Acad. Sci. USA 110 (2013) 11256–11260.
- [14] S. Shallcross, S. Sharma, E. Kandelaki, O.A. Pankratov, Electronic structure of turbostratic graphene, Phys. Rev. B Condensed Matter Mater. Phys. 81 (2010).
- [15] K. Hermann, Periodic overlayers and moiré patterns: Theoretical studies of geometric properties, J. Phys. Condensed Matter 24 (2012).
- [16] S.S. Sunku, et al., Photonic crystals for nano-light in moiré graphene superlattices, Science 362 (2018) 1153–1156.
- [17] Y. Zhang, Y. Kim, M.J. Gilbert, N. Mason, Magnetotransport in a strain superlattice of graphene, Appl. Phys. Lett. 115 (2019).
- [18] C.R. Woods, et al., Commensurate-incommensurate transition in graphene on hexagonal boron nitride, Nat. Phys. 10 (2014) 451–456.
- [19] X.-Q. Zheng, J. Lee, P.X.-L. Feng, Hexagonal boron nitride nanomechanical resonators with spatially visualized motion, Microsyst. Nanoeng. 3 (2017) 1–8.
- [20] M.A. Hossain, J. Yu, A.M. van der Zande, Realizing optoelectronic devices from crumpled two-dimensional material heterostructures, ACS Appl. Mater. Interf. 12 (2020) 48910–48916.
- [21] M.K. Blees, et al., Graphene kirigami, Nature 524 (2015) 204–207.
- [22] W. Lee, et al., Two-dimensional materials in functional three-dimensional architectures with applications in photodetection and imaging, Nature Commun. 9 (2018) 1–9.
- [23] Z. Liu, et al., Observation of Microscale Superlubricity in Graphite, Phys. Rev. Lett. 108 (2012) 205503–205505.
- [24] R. Ribeiro-Palau, et al., Twistable electronics with dynamically rotatable heterostructures, Science 361 (2018) 690–693.
- [25] Arend M. van der Zande, James C. Hone, Optical Materials: Inspired by strain, Nature Photonics 6 (2012) 804–806, https://doi.org/10.1038/ nphoton.2012.303.
- [26] Y. Zhang, Y.W. Tan, H.L. Stormer, P. Kim, Experimental observation of the quantum Hall effect and Berry's phase in graphene, Nature 438 (2005) 201–204.
- [27] K.S. Novoselov, et al., Two-dimensional gas of massless Dirac fermions in graphene, Nature 438 (2005) 197–200.
- [28] K.F. Mak, K.L. McGill, J. Park, P.L. McEuen, The valley Hall effect in MoS2 transistors, Science 344 (2014) 1489–1492.
- [29] J.R. Schaibley, et al., Valleytronics in 2D materials, Nature Rev. Mater. 1 (2016) 115–172.
- [30] C. Chakraborty, N. Vamivakas, D. Englund, Advances in quantum light emission from 2D materials, Nanophotonics (2019).
- [31] X. Liu, M.C. Hersam, 2D materials for quantum information science, Nature Rev. Mater. (2019).
- [32] A. Manchon, H.C. Koo, J. Nitta, S.M. Frolov, R.A. Duine, New perspectives for Rashba spin-orbit coupling, Nat. Mater. 14 (2015) 871–882.
- [33] B. Huang, et al., Electrical control of 2D magnetism in bilayer CrI3, Nat. Nanotechnol. 13 (2018) 544–548.
- [34] K.S. Burch, D. Mandrus, J.-G. Park, Magnetism in two-dimensional van der Waals materials, Nature 563 (2018) 47–52.
- [35] P. Ajayan, P. Kim, K. Banerjee, Two-dimensional van der waals materials, Phys. Today 69 (2016).
- [36] G. Iannaccone, F. Bonaccorso, L. Colombo, G. Fiori, Quantum engineering of transistors based on 2D materials heterostructures, Nat. Nanotechnol. 13 (2018) 100, 120.
- [37] G.H. Lee, et al., Flexible and transparent MoS2 field-effect transistors on hexagonal boron nitride-graphene heterostructures, ACS Nano 7 (2013) 7931–7936.
- [38] C.-H. Lee, et al., Atomically thin p-n junctions with van der Waals heterointerfaces, Nat. Nanotechnol. 9 (2014) 676-681.
- [39] Y. Gao, et al., High-speed electro-optic modulator integrated with grapheneboron nitride heterostructure and photonic crystal nanocavity, Nano Lett. 15 (2015) 2001–2005.

- [40] A.M. Van Der Zande, et al., Tailoring the electronic structure in bilayer molybdenum disulfide via interlayer twist, Nano Lett. 14 (2014) 3869–3875.
- [41] E. Koren, et al., Coherent commensurate electronic states at the interface between misoriented graphene layers, Nat. Nanotechnol. 11 (2016) 752–757.
- [42] T. Chari, R. Ribeiro-Palau, C.R. Dean, K. Shepard, Resistivity of rotated graphite-graphene contacts, Nano Lett. 16 (2016) 4477–4482.
- [43] C.R. Dean, et al., Hofstadter's butterfly and the fractal quantum Hall effect in moiré superlattices, Nature 497 (2013) 598–602.
- [44] Y. Cao, et al., Unconventional superconductivity in magic-angle graphene superlattices, Nature 556 (2018) 43–50.
- [45] K. Tran, et al., Evidence for moiré excitons in van der Waals heterostructures, Nature 567 (2019) 71–75.
- [46] E.M. Alexeev, et al., Resonantly hybridized excitons in moiré superlattices in van der Waals heterostructures, Nature 567 (2019) 81–86.
- [47] C. Jin, et al., Observation of moiré excitons in WSe2/WS2 heterostructure superlattices, Nature 567 (2019) 76–80.
- [48] C. Chen, et al., Performance of monolayer graphene nanomechanical resonators with electrical readout, Nat. Nanotechnol. 4 (2009) 861–867.
- [49] J.S. Bunch, et al., Electromechanical resonators from graphene sheets, Science 315 (2007) 490–493.
- [50] M. Jung, et al., Ghz nanomechanical resonator in an ultraclean suspended graphene p-n junction, Nanoscale 11 (2019) 4355–4361.
- [51] F. Ye, J. Lee, P.X.L. Feng, Electrothermally tunable graphene resonators operating at very high temperature up to 1200 k, Nano Lett. 18 (2018) 1678–1685.
- [52] S.N.R. Kazmi, A.Z. Hajjaj, M.A.A. Hafiz, P.M.F.J. Costa, M.I. Younis, Highly tunable electrostatic nanomechanical resonators, IEEE Trans. Nanotechnol. 17 (2018) 113–121.
- [53] J. Lee, et al., Electrically tunable single- and few-layer mos2 nanoelectromechanical systems with broad dynamic range, Sci. Adv. 4 (2018).
- [54] Z. Wang, P.X.-L. Feng, Dynamic range of atomically thin vibrating nanomechanical resonators, Appl. Phys. Lett. 104 (2014) 103109.
- [55] R. De Alba, et al., Tunable phonon-cavity coupling in graphene membranes, Nat. Nanotechnol. 11 (2016) 741–746.
- [56] S. Jiang, H. Xie, J. Shan, K.F. Mak, Exchange magnetostriction in twodimensional antiferromagnets, Nat. Mater. (2020).
- [57] H.-K. Li, et al., Valley optomechanics in a monolayer semiconductor, Nat. Photonics 13 (2019) 397–401.
- [58] R.A. Barton, et al., High, size-dependent quality factor in an array of graphene mechanical resonators, Nano Lett. 11 (2011) 1232–1236.
- [59] J. Lee, Z. Wang, K. He, J. Shan, P.X. Feng, High frequency MoS2 nanomechanical resonators, ACS Nano 7 (2013) 6086–6091.
- [60] A. Castellanos-Gomez, et al., Single-layer mos2 mechanical resonators, Adv. Mater. 25 (2013) 6719–6723.
- [61] A.M. Van Der Zande, et al., Large-scale arrays of single-layer graphene resonators, Nano Lett. 10 (2010) 4869–4873.
- [62] A. Eichler, et al., Nonlinear damping in mechanical resonators made from carbon nanotubes and graphene, Nat. Nanotechnol. 6 (2011) 339–342.
- [63] J.E.P. Güttinger, et al., Energy-dependent path of dissipation in nanomechanical resonators, Nat. Nanotechnol. 12 (2017) 631.
- [64] D. Garcia-Sanchez, et al., Imaging mechanical vibrations in suspended graphene sheets, Nano Lett. 8 (2008) 1399–1403.
- [65] D. Davidovikj, et al., Visualizing the motion of graphene nanodrums, Nano Lett. 16 (2016) 2768–2773.
- [66] Z. Wang, et al., Resolving and tuning mechanical anisotropy in black phosphorus via nanomechanical multimode resonance spectromicroscopy, Nano Lett. 16 (2016) 5394–5400. PMID: 27505636.
- [67] M. Will, et al., High quality factor graphene-based two-dimensional heterostructure mechanical resonator, Nano Lett. 17 (2017) 5950–5955.
- [68] F. Ye, J. Lee, P.X.-L. Feng, Atomic layer mos2-graphene van der waals heterostructure nanomechanical resonators, Nanoscale 9 (2017) 18208–18215.
- [69] S. Kim, J. Yu, A.M. van der Zande, Nano-electromechanical drumhead resonators from two-dimensional material bimorphs, Nano Lett. 18 (2018) 6686–6695.
- [70] S.K. Sahu, et al., Nanoelectromechanical resonators from high- t c superconducting crystals of bi 2 sr 2 ca 1 cu 2 $o_{8\delta}$, 2D Materials 6 (2019) 025027.
- [71] X. Liu, et al., Large arrays and properties of 3-terminal graphene nanoelectromechanical switches, Adv. Mater. 26 (2014) 1571–1576.
- [72] C. Chen, et al., Graphene mechanical oscillators with tunable frequency, Nat. Nanotechnol. 8 (2013) 923–927.
- [73] H. Tian, et al., Graphene-on-paper sound source devices, ACS Nano 5 (2011) 4878–4885. PMID: 21591811.
- [74] H. Tian, et al., Single-layer graphene sound-emitting devices: experiments and modeling, Nanoscale 4 (2012) 2272–2277.
- [75] J.W. Suk, K. Kirk, Y. Hao, N.A. Hall, R.S. Ruoff, Thermoacoustic sound generation from monolayer graphene for transparent and flexible sound sources, Adv. Mater. 24 (2012) 6342–6347.
- [76] Q. Zhou, A. Zettl, Electrostatic graphene loudspeaker, Appl. Phys. Lett. 102 (2013) 223109.
- [77] M.C. Lemme, et al., Nanoelectromechanical sensors based on suspended 2d materials, Research 2020 (2020) 8748602.
- [78] P. Weber, J. Güttinger, A. Noury, J. Vergara-Cruz, A. Bachtold, Force sensitivity of multilayer graphene optomechanical devices, Nature Commun. 7 (2016) 12496.
- [79] J.D. Teufel, T. Donner, M.A. Castellanos-Beltran, J.W. Harlow, K.W. Lehnert, Nanomechanical motion measured with an imprecision below that at the standard quantum limit, Nat. Nanotechnol. 4 (2009) 820–823.

- [80] J. Chaste, et al., A nanomechanical mass sensor with yoctogram resolution, Nat. Nanotechnol. 7 (2012) 301–304.
- [81] X. Fan, et al., Graphene ribbons with suspended masses as transducers in ultrasmall nanoelectromechanical accelerometers, Nature Electron. 2 (2019) 394–404.
- [82] A. Blaikie, D. Miller, B.J. Alemán, A fast and sensitive room-temperature graphene nanomechanical bolometer, Nature Commun. 10 (2019) 4726.
- [83] S. Kim, et al., Stochastic stress jumps due to soliton dynamics in two-dimensional van der Waals interfaces, Nano Lett. (2020) acs.nanolett.9b04619.
- [84] N. Morell, et al., Optomechanical measurement of thermal transport in twodimensional mose2 lattices, Nano Lett. (2019).
- [85] A. Islam, A. van den Akker, P.X.L. Feng, Anisotropic thermal conductivity of suspended black phosphorus probed by opto-thermomechanical resonance spectromicroscopy, Nano Lett. 18 (2018) 7683–7691.
- [86] S. Sengupta, H.S. Solanki, V. Singh, S. Dhara, M.M. Deshmukh, Electromechanical resonators as probes of the charge density wave transition at the nanoscale in nbse₂, Phys. Rev. B 82 (2010) 155432.
- [87] M. Šiškins, et al., Magnetic and electronic phase transitions probed by nanomechanical resonators, Nature Commun. 11 (2020) 2698.
- [88] V. Singh, et al., Coupling between quantum hall state and electromechanics in suspended graphene resonator, Appl. Phys. Lett. 100 (2012) 233103.
- [89] W. Chen, et al., Controllable fabrication of large-area wrinkled graphene on a solution surface, ACS Appl. Mater. Interf. 8 (2016) 10977–10984.
- [90] D. Davidovikj, et al., Ultrathin complex oxide nanomechanical resonators, Commun. Phys. 3 (2020) 163.
- [91] A.M. Eriksson, D. Midtvedt, A. Croy, A. Isacsson, Frequency tuning, nonlinearities and mode coupling in circular mechanical graphene resonators, Nanotechnology 24 (2013) 395702.
- [92] J.P. Mathew, R.N. Patel, A. Borah, R. Vijay, M.M. Deshmukh, Dynamical strong coupling and parametric amplification of mechanical modes of graphene drums, Nat. Nanotechnol. 11 (2016) 747.
- [93] P. Prasad, N. Arora, A.K. Naik, Parametric amplification in mos2 drum resonator, Nanoscale 9 (2017) 18299–18304.
- [94] R.J. Dolleman, et al., High-frequency stochastic switching of graphene resonators near room temperature, Nano Lett. 19 (2019) 1282–1288. PMID: 30681865.
- [95] D. Davidovikj, et al., Nonlinear dynamic characterization of two-dimensional materials, Nature Commun. 8 (2017) 1253.
- [96] J. Atalaya, J.M. Kinaret, A. Isacsson, Nanomechanical mass measurement using nonlinear response of a graphene membrane, EPL (Europhys. Lett.) 91 (2010) 48001.
- [97] J.-W. Jiang, H.S. Park, T. Rabczuk, Enhancing the mass sensitivity of graphene nanoresonators via nonlinear oscillations: the effective strain mechanism, Nanotechnology 23 (2012) 475501.
- [98] S.S.P. Nathamgari, et al., Nonlinear mode coupling and one-to-one internal resonances in a monolayer ws2 nanoresonator, Nano Lett. 19 (2019) 4052–4059. PMID: 31117759.
- [99] H.W.C. Postma, I. Kozinsky, A. Husain, M.L. Roukes, Dynamic range of nanotubeand nanowire-based electromechanical systems, Appl. Phys. Lett. 86 (2005) 223105.
- [100] X. Song, et al., Stamp transferred suspended graphene mechanical resonators for radio frequency electrical readout, Nano Lett. 12 (2012) 198–202.
- [101] A.W. Barnard, V. Sazonova, A.M. van der Zande, P.L. McEuen, Fluctuation broadening in carbon nanotube resonators, Proc. Nat. Acad. Sci. 109 (2012) 19093–19096.
- [102] P. Weber, J. Güttinger, I. Tsioutsios, D.E. Chang, A. Bachtold, Coupling graphene mechanical resonators to superconducting microwave cavities, Nano Lett. 14 (2014) 2854–2860.
- [103] N. Morell, et al., High quality factor mechanical resonators based on WSe2 monolayers, Nano Lett. 16 (2016) 5102–5108.
- [104] I.R. Storch, et al., Young's modulus and thermal expansion of tensioned graphene membranes, Phys. Rev. B 98 (2018) 085408.
- [105] S. De, A. van der Zande, N.R. Aluru, Intrinsic dissipation due to mode coupling in two-dimensional-material resonators revealed through a multiscale approach, Phys. Rev. Appl. 14 (2020) 034062.
- [106] R.A. Barton, et al., Photothermal self-oscillation and laser cooling of graphene optomechanical systems, Nano Lett. 12 (2012) 4681–4686.
- [107] J.A. Robinson, et al., Raman topography and strain uniformity of large-area epitaxial graphene, Nano Lett. 9 (2009) 964–968.
- [108] J.A. Robinson, et al., Correlating raman spectral signatures with carrier mobility in epitaxial graphene: a guide to achieving high mobility on the wafer scale, Nano Lett. 9 (2009) 2873–2876.
- [109] H. Li, et al., Optoelectronic crystal of artificial atoms in strain-textured molybdenum disulphide, Nature Commun. 6 (2015).
- [110] C. Palacios-Berraquero, et al., Large-scale quantum-emitter arrays in atomically thin semiconductors, Nature Commun. 8 (2017) 1–6.
- [111] V.S. Mangu, M. Zamiri, S.R. Brueck, F. Cavallo, Strain engineering, efficient excitonic photoluminescence, and exciton funnelling in unmodified MoS2nanosheets, Nanoscale 9 (2017) 16602–16606.
- [112] S. Bertolazzi, J. Brivio, A. Kis, Stretching and breaking of ultrathin MoS2, ACS Nano 5 (2011) 9703–9709.
- [113] M.R. Rosenberger, et al., Quantum calligraphy: writing single-photon emitters in a two-dimensional materials platform, ACS Nano 13 (2019) 904–912.
- [114] S.P. Koenig, N.G. Boddeti, M.L. Dunn, J.S. Bunch, Ultrastrong adhesion of graphene membranes, Nat. Nanotechnol. 6 (2011) 543–546.
- [115] D. Lloyd, et al., Adhesion, stiffness, and instability in atomically thin MoS 2Bubbles, Nano Lett. 17 (2017) 5329–5334.

- [116] G.H. Ahn, et al., Strain-engineered growth of two-dimensional materials, Nature Commun. 8 (2017) 1–8.
- [117] S.-W. Wang, et al., Thermally strained band gap engineering of transition-metal dichalcogenide bilayers with enhanced light-matter interaction toward excellent photodetectors, ACS Nano 11 (2017) 8768–8776.
- [118] G. Plechinger, et al., Control of biaxial strain in single-layer molybdenite using local thermal expansion of the substrate, 2D Materials 2 (2015) 015006.
- [119] M. Yankowitz, et al., Tuning superconductivity in twisted bilayer graphene, Science 363 (2019) 1059–1064.
- [120] T. Song, et al., Switching 2d magnetic states via pressure tuning of layer stacking, Nat. Mater. 18 (2019) 1298–1302.
- [121] Z.H. Ni, et al., Uniaxial strain on graphene: Raman spectroscopy study and bandgap opening, ACS Nano 2 (2008) 2301–2305.
- [122] T.M.G. Mohiuddin, et al., Uniaxial strain in graphene by Raman spectroscopy: G peak splitting, Grüneisen parameters, and sample orientation, Phys. Rev. B 79 (2009) 205433.
- [123] M. Huang, et al., Phonon softening and crystallographic orientation of strained graphene studied by raman spectroscopy, Proc. Nat. Acad. Sci. 106 (2009)
- [124] G. Tsoukleri, et al., Subjecting a graphene monolayer to tension and compression, small 5 (2009) 2397–2402.
- [125] H.J. Conley, et al., Bandgap engineering of strained monolayer and bilayer MoS 2, Nano Lett. 13 (2013) 3626–3630.
- [126] K. He, C. Poole, K.F. Mak, J. Shan, Experimental demonstration of continuous electronic structure tuning via strain in atomically thin mos2, Nano Lett. 13 (2013) 2931–2936.
- [2013] 2931–2936.
 [127] C. Rice, et al., Raman-scattering measurements and first-principles calculations of strain-induced phonon shifts in monolayer MoS₂, Phys. Rev. B 87 (2013) 081307.
- [128] O.B. Aslan, M. Deng, T.F. Heinz, Strain tuning of excitons in monolayer wse 2, Phys. Rev. B 98 (2018) 115308.
- [129] P. Gant, et al., A strain tunable single-layer MoS 2 photodetector, Mater. Today 27 (2019) 8–13.
- [130] Z. Liu, et al., Strain and structure heterogeneity in MoS 2 atomic layers grown by chemical vapour deposition, Nature Commun. 5 (2014).
- [131] T. Jiang, R. Huang, Y. Zhu, Interfacial sliding and buckling of monolayer graphene on a stretchable substrate, Adv. Funct. Mater. 24 (2013) 396–402.
- [132] L. Jiang, et al., Manipulation of domain-wall solitons in bi- and trilayer graphene, Nat. Nanotechnol. 13 (2018) 204–208.
- [133] J. Yu, S. Kim, E. Ertekin, A.M. van der Zande, Material-dependent evolution of mechanical folding instabilities in two-dimensional atomic membranes, ACS Appl. Mater. Interf. (2020) acsami.9b20909.
- [134] Z. Li, et al., Efficient strain modulation of 2D materials via polymer encapsulation, Nature Commun. 11 (2020) 1–8.
- [135] D. Lloyd, et al., Band gap engineering with ultralarge biaxial strains in suspended monolayer MoS 2. Nano Lett. 16 (2016) 5836–5841.
- [136] Y. Wang, et al., Strain-induced direct-indirect bandgap transition and phonon modulation in monolayer WS2, Nano Res. 8 (2015) 2562–2572.
- [137] J. Lee, Z. Wang, H. Xie, K.F. Mak, J. Shan, Valley magnetoelectricity in single-layer MoS2, Nat. Mater. 16 (2017) 887–892.
- [138] J.S. Bunch, et al., Impermeable atomic membranes from graphene sheets, Nano Lett. 8 (2008) 2458–2462.
- [139] P.Z. Sun, et al., Limits on gas impermeability of graphene, Nature 579 (2020) 229–232.
- [140] M. Guo, Y. Qian, H. Qi, K. Bi, Y. Chen, Experimental measurements on the thermal conductivity of strained monolayer graphene, Carbon 157 (2020) 185–190.
- [141] G. Wang, et al., Measuring interlayer shear stress in bilayer graphene, Phys. Rev. Lett. 119 (2017) 036101.
- [142] G. Wang, et al., Bending of multilayer van der Waals materials, Phys. Rev. Lett. 123 (2019) 116101.
- [143] K.A.N. Duerloo, Y. Li, E.J. Reed, Structural phase transitions in two-dimensional Mo-and W-dichalcogenide monolayers, Nature Commun. 5 (2014) 1–9.
- [144] J. Berry, S. Zhou, J. Han, D.J. Srolovitz, M.P. Haataja, Dynamic phase engineering of bendable transition metal dichalcogenide monolayers, Nano Lett. 17 (2017) 2473–2481
- [145] Y. Wang, et al., Structural phase transition in monolayer mote 2 driven by electrostatic doping, Nature 550 (2017) 487–491.
- [146] Y. Li, K.-A.N. Duerloo, K. Wauson, E.J. Reed, Structural semiconductor-tosemimetal phase transition in two-dimensional materials induced by electrostatic gating, Nature Commun. 7 (2016) 1–8.
- [147] S. Song, et al., Room temperature semiconductor-metal transition of mote2 thin films engineered by strain, Nano Lett. 16 (2016) 188–193.
- [148] S. Carr, S. Fang, P. Jarillo-Herrero, E. Kaxiras, Pressure dependence of the magic twist angle in graphene superlattices, Phys. Rev. B 98 (2018) 085144.
- [149] B.L. Chittari, N. Leconte, S. Javvaji, J. Jung, Pressure induced compression of flatbands in twisted bilayer graphene, Electron. Struct. 1 (2018) 015001.
- [150] N. Levy, et al., Strain-induced pseudo-magnetic fields greater than 300 Tesla in graphene nanobubbles, Science 329 (2010) 544–547.
- [151] M.A. Hossain, Y. Zhang, A.M. van der Zande, Strain engineering photonic properties in monolayer semiconductors through mechanically-reconfigurable wrinkling, in: C. Nielsen, D. Congreve (Eds.), Physical Chemistry of Semiconductor Materials and Interfaces XIX, vol. 11464, International Society for Optics and Photonics (SPIE), 2020, p. 1146404, https://doi.org/10.1117/ 12.2567539.
- [152] D.A. Sanchez, et al., Mechanics of spontaneously formed nanoblisters trapped by transferred 2D crystals, Proc. Nat. Acad. Sci. 115 (2018) 201801551.

- [153] E. Khestanova, F. Guinea, L. Fumagalli, A.K. Geim, I.V. Grigorieva, Universal shape and pressure inside bubbles appearing in van der Waals heterostructures, Nature Commun. 7 (2016) 1–10.
- [154] M.G. Harats, J.N. Kirchhof, M. Qiao, K. Greben, K.I. Bolotin, Dynamics and efficient conversion of excitons to trions in non-uniformly strained monolayer WS2, Nat. Photonics 14 (2020) 324–329.
- [155] H. Moon, et al., Dynamic exciton funneling by local strain control in a monolayer semiconductor, Nano Lett. 20 (2020) 6791–6797.
- [156] T.P. Darlington, et al., Imaging strain-localized excitons in nanoscale bubbles of monolayer WSe2 at room temperature, Nat. Nanotechnol. 15 (2020) 854–860.
- [157] Y. Zhang, et al., Strain modulation of graphene by nanoscale substrate curvatures: a molecular view, Nano Lett. 18 (2018) 2098–2104.
- [158] Z. Bi, N.F.Q. Yuan, L. Fu, Designing flat bands by strain, Phys. Rev. B 100 (2019) 035448.
- [159] J. Zang, et al., Multifunctionality and control of the crumpling and unfolding of large-area graphene, Nat. Mater. 12 (2013) 321–325.
- [160] Q. Wang, X. Zhao, A three-dimensional phase diagram of growth-induced surface instabilities, Sci. Rep. 5 (2015) 1–10.
- [161] L. Pocivavsek, et al., Stress and fold localization in thin elastic membranes, Science 320 (2008) 912–916.
- [162] P. Kim, M. Abkarian, H.A. Stone, Hierarchical folding of elastic membranes under biaxial compressive stress, Nat. Mater. 10 (2011) 952–957.
- [163] A.V. Thomas, et al., Controlled crumpling of graphene oxide films for tunable optical transmittance, Adv. Mater. 27 (2015) 3256–3265.
- [164] D. Rhee, et al., Soft skin layers enable area-specific, multiscale graphene wrinkles with switchable orientations, ACS Nano 14 (2020) 166–174.
- [165] J. Lee, et al., Switchable, tunable, and directable exciton funneling in periodically wrinkled ws2, Nano Lett. (2020).
- [166] J. Zang, C. Cao, Y. Feng, J. Liu, X. Zhao, Stretchable and high-performance supercapacitors with crumpled graphene papers, Sci. Rep. 4 (2014).
- [167] P. Kang, M.C. Wang, P.M. Knapp, S. Nam, Crumpled graphene photodetector with enhanced, strain-tunable, and wavelength-selective photoresponsivity, Adv. Mater. 28 (2016) 4639–4645.
- [168] S. Deng, V. Berry, Wrinkled, rippled and crumpled graphene: an overview of formation mechanism, electronic properties, and applications, Mater. Today 19 (2016) 197–212.
- [169] S. Deng, et al., Graphene wrinkles enable spatially defined chemistry, Nano Lett. 19 (2019) 5640–5646.
- [170] Z. Wang, et al., Wrinkled, wavelength-tunable graphene-based surface topographies for directing cell alignment and morphology, Carbon 97 (2016) 14–24
- [171] P.Y. Chen, M. Zhang, M. Liu, I.Y. Wong, R.H. Hurt, Ultrastretchable graphene-based molecular barriers for chemical protection, detection, and actuation, ACS Nano 12 (2018) 234–244.
- [172] J. Choi, et al., Hierarchical, dual-scale structures of atomically thin mos2 for tunable wetting, Nano Lett. 17 (2017) 1756–1761.
- [173] J. Leem, M.C. Wang, P. Kang, S. Nam, Mechanically self-assembled, threedimensional graphene-gold hybrid nanostructures for advanced nanoplasmonic sensors, Nano Lett. 15 (2015) 7684–7690.
- [174] Y. Zhao, et al., Plasmonic-enhanced Raman scattering of graphene on growth substrates and its application in SERS, Nanoscale 6 (2014) 13754–13760.
- [175] W. Ren, Y. Fang, E. Wang, A binary functional substrate for enrichment and ultrasensitive SERS spectroscopic detection of folic acid using graphene oxide/Ag nanoparticle hybrids, ACS Nano 5 (2011) 6425–6433.
- [176] K.S. Kim, et al., Large-scale pattern growth of graphene films for stretchable transparent electrodes, Nature 457 (2009) 706–710.
- [177] X. Wang, L. Zhi, K. Müllen, Transparent, conductive graphene electrodes for dyesensitized solar cells, Nano Lett. 8 (2008) 323–327.
- [178] N. Petrone, I. Meric, J. Hone, K.L. Shepard, Graphene field-effect transistors with gigahertz-frequency power gain on flexible substrates, Nano Lett. 13 (2013) 121–125.
- [179] B.J. Kim, et al., High-performance flexible graphene field effect transistors with ion gel gate dielectrics, Nano Lett. 10 (2010) 3464–3466.
- [180] C.-C. Lu, Y.-C. Lin, C.-H. Yeh, J.-C. Huang, P.-W. Chiu, High mobility flexible graphene field-effect transistors with self-healing gate dielectrics, ACS Nano 6 (2012) 4469–4474.
- [181] D. De Fazio, et al., High responsivity, large-area graphene/mos2 flexible photodetectors, ACS Nano 10 (2016) 8252–8262.
- [182] H. Kim, J.-H. Ahn, Graphene for flexible and wearable device applications, Carbon 120 (2017) 244–257.
- [183] D. Akinwande, N. Petrone, J. Hone, Two-dimensional flexible nanoelectronics, Nature Commun. 5 (2014).
- [184] T. Georgiou, et al., Vertical field-effect transistor based on graphene-ws 2 heterostructures for flexible and transparent electronics, Nature Nanotechnol. 8 (2013) 100.
- [185] J. Lee, et al., High-performance current saturating graphene field-effect transistor with hexagonal boron nitride dielectric on flexible polymeric substrates, IEEE Electron Device Lett. 34 (2013) 172–174.
 [186] C. H. Vah, et al., Circhest, flexible graphene transistors for microwave integrated.
- [186] C.H. Yeh, et al., Gigahertz flexible graphene transistors for microwave integrated circuits, ACS Nano 8 (2014) 7663–7670.
- [187] J.A. Rogers, T. Someya, Y. Huang, Materials and mechanics for stretchable electronics, Science 327 (2010) 1603–1607.
- [188] M.T. Hwang, et al., Ultrasensitive detection of nucleic acids using deformed graphene channel field effect biosensors, Nature Commun. 11 (2020) 1543.
- [189] J. Leem, et al., Crack-assisted, localized deformation of van der waals materials for enhanced strain confinement, 2D Materials 6 (2019) 044001.

- [190] S. Yang, et al., Tuning the optical, magnetic, and electrical properties of rese2 by nanoscale strain engineering, Nano Lett. 15 (2015) 1660–1666.
- [191] M.Z. Miskin, et al., Graphene-based bimorphs for micron-sized, autonomous origami machines, in: Proc. Nat. Acad. Sci., 2018, 201712889.
- [192] S.J. Callens, A.A. Zadpoor, From flat sheets to curved geometries: Origami and kirigami approaches, Mater. Today 21 (2018) 241–264.
- [193] G.P. Choi, L.H. Dudte, L. Mahadevan, Programming shape using kirigami tessellations, Nat. Mater. 18 (2019) 999–1004.
- [194] D. Yang, et al., Paper-cut flexible multifunctional electronics using mos2 nanosheet, Nanomaterials 9 (2019).
- [195] S. Lim, et al., Assembly of foldable 3D microstructures using graphene hinges, Adv. Mater. 32 (2020) 2001303.
- [196] W. Xu, et al., Reversible MoS 2 Origami with Spatially Resolved and Reconfigurable Photosensitivity, Nano Lett. 19 (2019) 7941–7949.
- [197] T. Deng, et al., Self-folding graphene-polymer bilayers, Appl. Phys. Lett. 106 (2015).
- [198] W. Xu, D.H. Gracias, Soft three-dimensional robots with hard two-dimensional materials, ACS Nano 13 (2019) 4883–4892.
- [199] M.Z. Miskin, et al., Electronically integrated, mass-manufactured, microscopic robots, Nature 584 (2020) 557–561.
- [200] F. Wu, T. Lovorn, A.H. Macdonald, Topological exciton bands in Moiré heterojunctions, Phys. Rev. Lett. 118 (2017) 1–6.
- [201] M. Peyrard, S. Aubry, Critical behaviour at the transition by breaking of analyticity in the discrete frenkel-kontorova model, J. Phys. C: Solid State Phys. 16 (1983) 1593–1608.
- [202] M. Hirano, K. Shinjo, R. Kaneko, Y. Murata, Anisotropy of frictional forces in muscovite mica, Phys. Rev. Lett. 67 (1991) 2642–2645.
- [203] M. Hirano, K. Shinjo, Atomistic locking and friction, Phys. Rev. B 41 (1990) 11837–11851.
- [204] C. Donnet, T. Le Mogne, J. Martin, Superlow friction of oxygen-free mos2 coatings in ultrahigh vacuum, Surf. Coat. Technol. 62 (1993) 406–411.
- [205] K. Shinjo, M. Hirano, Dynamics of friction: superlubric state, Surf. Sci. 283 (1993) 473–478.
- [206] O. Hod, E. Meyer, Q. Zheng, M. Urbakh, Structural superlubricity and ultralow friction across the length scales, Nature 563 (2018) 485–492.
- [207] J.M. Martin, A. Erdemir, Superlubricity: Friction's vanishing act, Phys. Today 71 (2018).
- [208] O. Zwörner, H. Hölscher, U. Schwarz, R. Wiesendanger, The velocity dependence of frictional forces in point-contact friction, Appl. Phys. A: Mater. Sci. Process. 66 (1998) S263–S267.
- [209] A. Erdemir, O.L. Eryilmaz, G. Fenske, Synthesis of diamondlike carbon films with superlow friction and wear properties, J. Vac. Sci. Technol. A: Vac. Surfaces Films 18 (2000) 1987–1992.
- [210] J.M. Martin, C. Donnet, T. Le Mogne, T. Epicier, Superlubricity of molybdenum disulphide, Phys. Rev. B 48 (1993) 10583–10586.
- [211] L. Scandella, et al., Tribology of ultra-thin MoS2 platelets on mica: studies by scanning force microscopy, Thin Solid Films 240 (1994) 101–104.
- [212] C. Lee, et al., Elastic and frictional properties of graphene, Phys. Status Solidi (b) 246 (2009) 2562–2567.
- [213] H. Lee, N. Lee, Y. Seo, J. Eom, S. Lee, Comparison of frictional forces on graphene and graphite, Nanotechnology 20 (2009) 325701.
- [214] M.R. Vazirisereshk, et al., Origin of nanoscale friction contrast between supported graphene, MoS 2, and a graphene/MoS 2 heterostructure, Nano Lett. 19 (2019) 5496–5505.
- [215] M. Dienwiebel, et al., Superlubricity of graphite, Phys. Rev. Lett. 92 (2004) 126101.
- [216] Y. Shibuta, J.A. Elliott, Interaction between two graphene sheets with a turbostratic orientational relationship, Chem. Phys. Lett. 512 (2011) 146–150.
- [217] B.J. Irving, P. Nicolini, T. Polcar, On the lubricity of transition metal dichalcogenides: An: ab initio study, Nanoscale 9 (2017) 5597–5607.
- [218] H. Li, et al., Superlubricity between MoS 2 Monolayers, Adv. Mater. 29 (2017) 1701474.
- [219] L. Wang, et al., Superlubricity of a graphene/MoS 2heterostructure: a combined experimental and DFT study, Nanoscale 9 (2017) 10846–10853.
- [220] H. Yoo, et al., Atomic reconstruction at van der Waals interface in twisted bilayer graphene, Nat. Mater. 18 (2018).
 [221] N.R. Finney, et al., Tunable crystal symmetry in graphene-boron nitride
- heterostructures with coexisting moiré superlattices, Nat. Nanotechnol. 14 (2019).

 [222] D. Mandelli, I. Leven, O. Hod, M. Urbakh, Sliding friction of graphene/hexagonal
- -boron nitride heterojunctions: A route to robust superlubricity, Sci. Rep. 7 (2017) 1–10.
- [223] Y. Song, et al., Robust microscale superlubricity in graphite/ hexagonal boron nitride layered heterojunctions, Nat. Mater. 17 (2018) 1–8.
- [224] M. Liao, et al., Twist angle-dependent conductivities across MoS2/graphene heterojunctions, Nature Commun. 9 (2018) 1–6.
- [225] L. Brown, et al., Twinning and twisting of tri- and bilayer graphene, Nano Lett. 12 (2012) 1609–1615. PMID: 22329410.
 [226] Y. Yang, et al., Stacking Order in Graphite Films Controlled by van der Waals
- Technology, Nano Lett. (2019) acs.nanolett.9b03014.

 [227] A. Weston, et al., Atomic reconstruction in twisted bilayers of transition metal
- dichalcogenides, Nat. Nanotechnol. 15 (2020) 592–597.

 [228] E. Koren, U. Duerig, Moiré scaling of the sliding force in twisted bilayer graphene, Phys. Rev. B 94 (2016) 45401–45411.
- [229] S. Ge, et al., Interlayer transport through a graphene/rotated boron nitride/ graphene heterostructure, Phys. Rev. B 95 (2017) 1–9.

- [230] A. Summerfield, et al., Moiré-modulated conductance of hexagonal boron nitride tunnel barriers, Nano Lett. 18 (2018) 4241–4246. PMID: 29913062.
- [231] A. Mishchenko, et al., Twist-controlled resonant tunnelling in graphene/boron nitride/graphene heterostructures, Nat. Nanotechnol. 9 (2014) 808–813.
- [232] L. Huder, et al., Electronic spectrum of twisted graphene layers under heterostrain, Phys. Rev. Lett. 120 (2018) 156405.
- [233] D. Edelberg, H. Kumar, V. Shenoy, H. Ochoa, A.N. Pasupathy, Tunable strain soliton networks confine electrons in van der waals materials, Nat. Phys. (2020).
- [234] T. Peña, et al., Strain engineering 2d mos_2 with thin film stress capping layers (2020). 2009.10626.
- [235] K. Kang, et al., High-mobility three-atom-thick semiconducting films with wafer-scale homogeneity, Nature 520 (2015) 656–660.
- [236] J. Gao, et al., Aging of transition metal dichalcogenide monolayers, ACS Nano (2016).
- [237] H. Gao, et al., Tuning electrical conductance of mos2monolayers through substitutional doping, Nano Lett. (2020).
- [238] L. Wang, et al., One-dimensional electrical contact to a two-dimensional material, Science 342 (2013) 614–617.
- [239] Y. Huang, et al., Reliable exfoliation of large-area high-quality flakes of graphene and other two-dimensional materials, ACS Nano (2015).
- [240] F. Liu, et al., Disassembling 2D van der Waals crystals into macroscopic monolayers and reassembling into artificial lattices, Science (2020).
- [241] Y. Huang, et al., Universal mechanical exfoliation of large-area 2D crystals, Nature Commun. (2020).

- [242] K. Kang, et al., Layer-by-layer assembly of two-dimensional materials into wafer-scale heterostructures, Nature (2017).
- [243] E.J. Telford, et al., Via method for lithography free contact and preservation of 2D materials, Nano Lett. (2018).
- [244] Y. Liu, et al., Approaching the Schottky-Mott limit in van der Waals metal-semiconductor junctions, Nature (2018).
- [245] C.M. Went, et al., A new metal transfer process for van der Waals contacts to vertical Schottky-junction transition metal dichalcogenide photovoltaics, Sci. Adv. (2019).
- [246] J. Son, et al., Atomically precise graphene etch stops for three dimensional integrated systems from two dimensional material heterostructures, Nature Commun. 9 (2018) 1–9.
- [247] X. Huang, L. Lin, Q. Zheng, Theoretical study of superlubric nanogenerators with superb performances, Nano Energy 70 (2020) 104494.
- [248] M. Luo, Z. Zhang, B.I. Yakobson, Tunable gigahertz oscillators of gliding incommensurate bilayer graphene sheets, J. Appl. Mech. 80 (2013) 040906.
- [249] S. Young Kim, S.-Y. Cho, K.-S. Kim, J. Won Kang, Developing nanoscale inertial sensor based on graphite-flake with self-retracting motion, Physica E 50 (2013) 44, 50
- [250] U.T. Duerig, A.W. Knoll, E. Koren, E. Loertscher, Electromechanical switching device with electrodes having 2d layered materials with distinct functional areas (2020). US Patent 10,546,708.